CHAPTER 4

SURFACE SECOND HARMONIC GENERATION STUDIES OF SINGLE CRYSTAL METAL SURFACES

G. L. Richmond and R. A. Bradley
Department of Chemistry
University of Oregon
Eugene, OR 97403, USA

Contents

1. Introduction

Over the past decade, our understanding of the atomic and electronic structure of metal surfaces examined under UHV conditions has improved significantly, aided by the proliferation of powerful electron spectroscopic techniques. Unfortunately, parallel elucidation of the detailed surface structure at the metal/electrolyte interface has not followed suit, largely because of the lack of suitable techniques for making comparable measurements *in situ*. This lag is understandable if one considers the difficulties, both theoretical and experimental, in treating the metal/electrolyte interface. Most UHV compatible techniques are not transferable to solution with the exception of X-ray grazing incidence studies and scanning tunneling microscopy measurements which have mainly focused on geometric surface structure. Second harmonic generation (SHG) which is the focus of this review has the potential to be a very simple means of measuring both surface electronic and geometric structure. It is ideal for studies of buried interfaces because of the inherent surface specificity and its versatility for studying surfaces in a variety of environments.

The fundamental issues to all of these electrochemical measurements are how the presence of the electrolyte solution and resulting double layer alter the surface properties as known from UHV studies. Are single crystal surfaces well ordered in the presence of the electrolyte and how does this surface order vary with applied field? How do molecules and electrodeposited overlayers align with the surface lattice? Surface reconstruction is another area which has been thoroughly explored in UHV but not in solution. In terms of the spectroscopy of the surface, what correlation if any exists between the electronic structure of surfaces in solution and the surface structure measured in UHV? Perhaps more important to electrochemists, how do the electronic properties of the metal surface vary with the applied potential? Since surface electronic structure for clean surfaces in UHV can be extremely sensitive to the presence of even submonolayer amounts of adsorbates, the contended persistence of surface states in the presence of aqueous electrolyte often receives skepticism. Intrinsic surface states and surface modified continuum bands, both consequences of the truncation of the periodic crystal lattice, are often invoked in investigations of optical properties of metals in solution. However, without compelling and unambiguous experimental confirmation these assignments are speculative, particularly when extended to extrinsic surface states

induced by the presence of defects, adsorbates or the applied field. Over the last decade, the participation of both crystal-induced (intrinsic) surface states and image potential (extrinsic) states has been invoked to account for potential-dependent features observed in the linear electroreflectance (ER) from a range of low index crystal faces of noble metal electrode surfaces. However, the incompatibility of ER to surfaces in UHV limits this analysis.

Just as there are questions which have arisen with regards to surface structure, there are equally compelling questions about the origin of the SH response from metal surfaces. Performing comparative SHG studies of surfaces in solution and in UHV can provide valuable information which can otherwise not be obtained from UHV experiments alone. In the electrochemical measurements one has the added dimension of being able to systematically vary the applied potential and surface charge by using simple potentiostatic methods. Because the electric field that develops at the surface is localized to the Thomas–Fermi screening length, one can test the surface sensitivity of the nonlinear technique by simple variation of the applied potential. If one uses appropriate surface preparation procedures and with ultraclean solutions, the issue of surface cleanliness which has previously been cited as a problem in electrochemical studies can be minimized.

The focus of the review will be on SHG from single crystal noble metal surfaces. These Cu, Ag and Au surfaces have been studied in the most detail. The well-known characteristics of the geometric and electronic structure of these metals make them model systems for examining the fundamental electrochemical and nonlinear optical issues outlined above. The focus will be on metal/electrolyte measurements performed *in situ*, and UHV measurements as they pertain to understanding the solution data. Primarily two types of experiments will be discussed, the first of which involve measuring the spectroscopy of the surface by variation of the incident wavelength and collecting the corresponding SH response. In the second type of measurements the incident wavelength is fixed and the crystal surface is rotated azimuthally. The resulting SH response is then a representation of the symmetry of the surface region and also provides valuable information of the phase of the SH response. The review will begin with a discussion of theoretical aspects which pertain to the analysis of the experimental data. This will be followed by a brief discussion of the important experimental parameters used in the measurements presented

in the remainder of the chapter. The electrochemical studies will primarily focus on very simple nonfaradaic processes. For a more comprehensive overview of SHG involving electron transfer processes including metal deposition and oxidation and reduction cycles, the reader is referred other references.[1–4]

2. Theoretical Considerations

This section begins with a general description of the nonlinear surface second harmonic (SH) response and a discussion of the source terms for the second-order polarization induced in a medium, including both surface and bulk contributions. For a more detailed description, refer to chapter XX. The phenomenological theories which relate to the effect of the sample symmetry on the SH response will follow. Finally, a brief description of the electrochemical interface previews a description of the coupling of the second-order response to the charging of the metal/electrolyte interface.

2.1. *Optical Nonlinearity: Anharmonic Oscillator Model*

The metals examined can be viewed as a collection of charged particles, namely the electrons and the respective ion cores. When an electromagnetic (EM) wave of light passes through such a medium, the ion cores feel a force in the direction of the electric field and the electrons a force in the opposite direction. In the presence of an electric field the electrons in the metallic conductor move freely, giving rise to an electrical current. Since the electromagnetic wave varies sinusoidally at an optical frequency ($\sim 10^{14}$–10^{15} Hz) this field induces an oscillating current in the metal. This complex response to the EM field is the polarization induced in the medium (metal), which itself gives rise to a new EM wave. In the case of dielectric materials (such as solvated ions in an electrolytic solution) the electrons are bound but the charge distribution of a dielectric will also adjust in response to the presence of an EM wave and become polarized albeit to a lesser extent than the charge distribution of a conductor. In both cases, the motion of the charged particles induced by the electromagnetic light waves creates oscillating dipoles or multipoles.

Since the positively charged particles have large masses, the interaction of the optical field with the medium can be described by the motion of the electron in an anharmonic potential in the usual mechanical ball and spring analogy[5]:

$$m\left[\frac{d^2x}{dt^2}+2\Gamma\frac{dx}{dt}+\Omega^2x-\left(\xi^{(2)}x^2+\xi^{(3)}x^3+\ldots\right)\right]=-eE(t)\,, \quad (1)$$

where x is the displacement from the mean position, Ω is the resonance frequency, Γ is the damping constant and $\xi^{(2)}$ and $\xi^{(3)}$ are two constants describing the anharmonic response. The first three terms in the brackets describe the (linear) harmonic motion of an electron exerted by the driving force ($-eE(t)$), the applied field. The linear harmonic response can be used to describe the familiar linear optical properties of a medium. However, the linear-dependence of the electron's response is a valid approximation only if the displacement x is small. In the case of high field strengths that are required for second harmonic generation, the displacement is large and the restoring force is significantly nonlinear. In the mechanical analogy, the additional anharmonic restoring force is $m(\xi^{(2)}x^2+\xi^{(3)}x^3+\ldots)$. Provided these anharmonic terms are small relative to the harmonic term, one can solve Eq. (1) to successive orders of approximation by expressing the displacement, or polarization, as a power series in the field $E(t)$. For a macroscopic system of many electrons, the analogous treatment expresses the expansion of the (dipole) polarization in the following form:

$$\mathbf{P}(t)=\varepsilon_0\left(\chi^{(1)}\mathbf{E}(t)+\chi^{(2)}\mathbf{E}^2(t)+\chi^{(3)}\mathbf{E}^3(t)+\ldots\right), \quad (2)$$

where $\chi^{(1)}$ represents the linear susceptibility, and the terms $\chi^{(2)}$, $\chi^{(3)}$, ... are the second- and third-order nonlinear susceptibilities of the medium.

The simple description of the local electric dipole response using the anharmonic oscillator model is a starting point, but higher order sources are appreciable in some second-order processes. When the electromagnetic field polarizes a medium, this interaction is governed by Maxwell's equations and the constitutive relations. When the polarized media is a metal, the charge density $\rho(r,t)$ and current $J(r,t)$ density are considered as the sources of the magnetic and electric field and are related by the law of charge conservation[6]:

$$\nabla\cdot J+\partial\rho/\partial t=0\,. \quad (3)$$

The relationship between the induced current density $J(r,t)$ in the medium and the general polarization P is just the following:

$$J=\partial P/\partial t\,. \quad (4)$$

If the polarization and charge density are known, an expression for the wave equation can be found, using the appropriate boundary conditions. However, solutions are not usually found easily and source terms can rarely be determined exactly.

A general description of the second-order polarization that gives rise to second harmonic generation is usually expressed by a series of multipole terms[7,8]:

$$P^{(2)}_{\text{eff}}(2\omega) = P^{(2)}(2\omega) - \nabla \cdot \vec{Q}^{(2)}(2\omega) + \frac{c}{i2\omega}\nabla \times M^{(2)}(2\omega)\,, \tag{5}$$

where $P^{(2)}$, $\vec{Q}^{(2)}$, and $M^{(2)}$ describe the electric-dipole polarization, electric-quadrupole polarization and magnetic-dipole polarization respectively. Up to the first derivative in $P^{(2)}_{\text{eff}}$, the three polarization sources are the following:

$$P^{(2)}(2\omega) = \vec{\vec{\chi}}^{D} : E(\omega)E(\omega) + \vec{\vec{\chi}}^{P} : E(\omega)\nabla E(\omega)\,, \tag{6}$$

$$Q^{(2)}(2\omega) = \vec{\vec{\chi}}^{Q} : E(\omega)E(\omega)\,, \tag{7}$$

$$M^{(2)}(2\omega) = \vec{\vec{\chi}}^{M} : E(\omega)E(\omega)\,. \tag{8}$$

In the bulk of centrosymmetric media, the first term of (6) and the contribution from $M^{(2)}$ (Eq. (8)) vanish.[8] Therefore, the bulk nonlinear polarization takes the form:

$$P^{(2)}_{\text{bulk}}(2\omega) = \vec{\vec{\chi}}^{P} : E(\omega)\nabla E(\omega) - \nabla \cdot \left[\vec{\vec{\chi}}^{Q} : E(\omega)E(\omega)\right]\,, \tag{9}$$

where a bulk contribution in both terms arises from the gradient in the field $E(\omega)$. Since the penetration depth in metals (~ 100 Å for the noble metals) is much smaller than the spatial variation of the field ($\sim 10\,000$ Å for optical frequencies), this contribution is small under nonresonant conditions.[9] Interestingly, there is also a surface contribution from the second term to the bulk nonlinear polarization arising from the discontinuity in $\vec{\vec{\chi}}^{Q}$ across the interface. However, this contribution is not sensitive to the surface conditions as it only depends on the bulk quadrupolar nonlinear susceptibilities.

At the surface the inversion symmetry is broken, giving rise to electric dipole and magnetic dipole source terms. Further, due to the electric field

discontinuity in the direction normal to the interface, electric quadrupole contribution can arise and the full expression for the surface contribution to the nonlinear polarization can be expressed as the following:

$$P^{(2)}_{\text{surface}}(2\omega) = \vec{\chi}^{D} : E(\omega)E(\omega) + \vec{\chi}^{P} : E(\omega)\nabla E(\omega) - \vec{\chi}^{Q} : \nabla E(\omega)E(\omega) + \frac{c}{i2\omega}\nabla \times \left[\vec{\chi}^{M} : E(\omega)E(\omega)\right] , \tag{10}$$

where the second and third terms only contribute to the surface response if either the fundamental or SH polarization is normal to the surface.

The full expression for the induced polarization in the medium, $P^{(2)}_{\text{eff}}$, including both surface and bulk contributions is the following:

$$P^{(2)}_{\text{eff}}(2\omega) = \vec{\chi}^{D} : E(\omega)E(\omega) + \vec{\chi}^{P} : E(\omega)\nabla E(\omega) - \nabla\vec{\chi}^{Q} : E(\omega)E(\omega) - \vec{\chi}^{Q} : \nabla E(\omega)E(\omega) + \frac{c}{i2\omega}\nabla \times \left[\vec{\chi}^{M} : E(\omega)E(\omega)\right] . \tag{11}$$

As mentioned above, the first two terms are electric dipole in nature, the third and fourth describe the electric quadrupole contribution and the last term the magnetic dipole contribution. Although surface contributions to the SH response from the magnetic dipole source term have been observed,[10] they should not be a factor in the studies presented here and are neglected. Under the electric dipole approximation, the second-order response vanishes in the bulk of centrosymmetric media and is allowed only at the interface where the inversion symmetry is broken. The presence of the interface not only creates a structural discontinuity, but a field discontinuity in the normal component of $E(\omega)$, as can be easily derived from Maxwell's equations. Since the tangential components of the incident electric field are continuous across the interface, all terms in Eq. (10) involving a gradient can be neglected when describing an in-plane surface response and only the first term should be considered. However, if either the driving fields or the SH polarization under consideration contains a field component normal to the surface, then there will be contributions from the higher order terms to the surface response.

As a consequence SHG derives its surface sensitivity from not only the dipole allowed surface terms, but higher order (quadrupole) terms which are inseparable from the dipole terms. For the systems under consideration here, one can express the induced nonlinear surface polarization in terms

of an effective susceptibility in the following manner:

$$P^{(2)}_{\text{eff}}(2\omega) = \vec{\vec{\chi}}_{\text{eff}} : E(\omega)E(\omega)\,, \tag{12}$$

where $\vec{\vec{\chi}}_{\text{eff}}$ is the second-order susceptibility tensor reflecting the optical as well as the symmetry properties of the surface layer. The tensorial properties of $\vec{\vec{\chi}}_{\text{eff}}$ can be exploited: If the SH intensity is recorded as a function of azimuthal angle of rotation, the variation in intensity reflects the overall symmetry of the surface.

2.2. *Rotational Anisotropy in the SH Response from Single Crystal Surfaces*

A tensorial expression for the second-order polarization can be written as the following:

$$\begin{pmatrix} P_x(2\omega) \\ P_y(2\omega) \\ P_z(2\omega) \end{pmatrix} = \begin{pmatrix} \chi_{xxx} & \chi_{xyy} & \chi_{xzz} & \chi_{xyz} & \chi_{xxz} & \chi_{xxy} \\ \chi_{yxx} & \chi_{yyy} & \chi_{yzz} & \chi_{yyz} & \chi_{yxz} & \chi_{yxy} \\ \chi_{zxx} & \chi_{zyy} & \chi_{zzz} & \chi_{zyz} & \chi_{zxz} & \chi_{zxy} \end{pmatrix} \times \begin{pmatrix} E_x(\omega)E_x(\omega) \\ E_y(\omega)E_y(\omega) \\ E_z(\omega)E_z(\omega) \\ 2E_y(\omega)E_z(\omega) \\ 2E_x(\omega)E_z(\omega) \\ 2E_x(\omega)E_y(\omega) \end{pmatrix}. \tag{13}$$

This is the general expression describing the interaction of the two EM driving fields being coupled through a dyadic product. Since the induced polarization is invariant with respect to an interchange of the two EM field components, the nonlinear field vector in Eq. (13) contains only 6 elements of the 9 possible permutations and the last two indices in each tensor element χ_{ijk} are interchangeable. As mentioned above, the components of the $\chi^{(2)}$ tensor reflect the symmetry of the interface. Only in the case of C_1 symmetry are all 18 independent elements of $\chi^{(2)}$ nonzero, and higher symmetries lead to a reduction in the number of independent and non-zero tensor elements.

Most of the work presented in this review has been performed on the (111) plane of the fcc noble metal surfaces. Well-defined surfaces of this

geometry have C_{3v} symmetry if at least two layers of the surface are considered. When the tensor in Eq. (13) is transformed by the symmetry operations that comprise C_{3v} symmetry (three vertical mirror planes and a threefold rotation axis) simple algebraic relationships are found that determine which of the tensor elements are independent and non-zero. The transformation rule for third rank tensors is the following[11]:

$$\chi_{ijk} = \sum_{l,m,n} R_{il} R_{jm} R_{kn} \chi_{lmn} \,, \tag{14}$$

where R is the symmetry operator. Transforming $\chi^{(2)}$ by the three vertical mirror planes and the threefold rotation axis reduces the 18 independent tensor elements to the following four: χ_{xxx} $(= -\chi_{xyy} = -\chi_{yxy})$, χ_{zxx} $(= \chi_{zyy})$, χ_{xxz} $(= \chi_{yyz})$, and χ_{zzz}. Shown below in Eq. (15) is the resulting expression for the $\chi^{(2)}$ tensor under C_{3v} symmetry:

$$\chi^{(2)} = \begin{pmatrix} \chi_{xxx} & -\chi_{xxx} & 0 & 0 & \chi_{xxz} & 0 \\ 0 & 0 & 0 & \chi_{xxz} & 0 & -\chi_{xxx} \\ \chi_{zxx} & \chi_{zxx} & \chi_{zzz} & 0 & 0 & 0 \end{pmatrix} . \tag{15}$$

In many of the experiments, the single crystal surface is rotated about its azimuthal angle (ϕ) and the SH response is analyzed with respect to the beam coordinates. Therefore, one needs to transform $\chi^{(2)}$ from crystal coordinates into beam coordinates, as shown in Fig. 1, with the appropriate transformation operations. This transformation, using the rule in Eq. (14) requires a mapping of the polarization from the crystal (x, y, z) to beam (k, s, z) coordinates, with the following transformation operator R:

$$R_{il} = \begin{pmatrix} \cos(\phi) & \sin(\phi) & 0 \\ -\sin(\phi) & \cos(\phi) & 0 \\ 0 & 0 & 1 \end{pmatrix} , \tag{16}$$

where ϕ is defined as the angle between the x- and k-axes. The azimuthal angle ϕ is defined as the angle between the $[2\bar{1}\bar{1}]$ direction on the (111) face and the projection of the incident wave vector parallel to the surface. In this transformation, p-polarization in beam coordinates is expressed as k, the in-plane component, and z, the out of plane component, in crystal coordinates. The transformation introduces an azimuthal dependence to

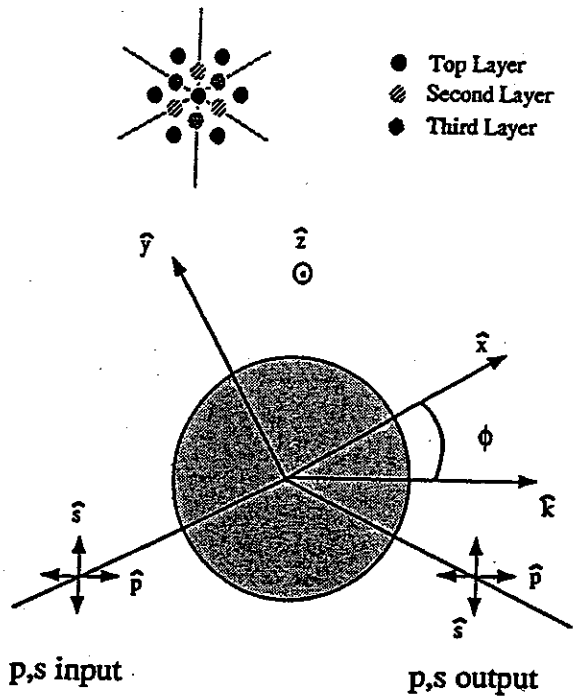

Fig. 1. A schematic of the beam and crystal coordinate systems for surface second harmonic generation. Also shown is a representation of the C_{3v} symmetry of the (111) face of a fcc metal.

the surface response, as measured in the beam coordinated system, and is shown in the following expression:

$$\chi^{(2)}_{\text{beam}} = \begin{pmatrix} \chi_{xxx}\cos(3\phi) & -\chi_{xxx}\cos(3\phi) & 0 & 0 & \chi_{xxz} & \chi_{xxx}\sin(3\phi) \\ \chi_{xxx}\sin(3\phi) & \chi_{xxx}\sin(3\phi) & 0 & \chi_{xxz} & 0 & -\chi_{xxx}\cos(3\phi) \\ \chi_{zxx} & \chi_{zxx} & \chi_{zzz} & 0 & 0 & 0 \end{pmatrix}, \tag{17}$$

where in this expression each tensor element of $\chi^{(2)}_{\text{beam}}$ (in beam coordinates) is written in terms of the surface susceptibility elements (in crystal coordinates).

Most of the SHG measurements presented in this work are obtained with *p*-polarized input light and either *p*- or *s*-polarized second harmonic light. As shown in Fig. 1, *p*-polarization refers to the polarization vector of the light residing in the plane of incidence, whereas the polarization vector for *s*-polarization is normal to the plane of incidence. A phenomenological theory of the azimuthal dependence of optical second harmonic generation from cubic media has been given by Tom[12] and Sipe.[13] In this model, the

second harmonic intensity from a [111] surface as a function of azimuthal rotation is described by the following expressions:

$$I_{p,p}^{(2\omega)}(\phi) = \left|a^{(\infty)} + c^{(3)}\cos(3\phi)\right|^2, \tag{18}$$

$$I_{p,s}^{(2\omega)}(\phi) = \left|b^{(3)}\sin(3\phi)\right|^2, \tag{19}$$

where the subscripts refer to the polarizations of the fundamental and SH light, respectively. The complex coefficients $a^{(\infty)}$, $b^{(3)}$, and $c^{(3)}$ contain the surface dipole susceptibility elements, χ_{ijk}, any contribution from higher order bulk susceptibility terms, γ and ζ, and the appropriate Fresnel factors. The complex coefficient $a^{(\infty)}$ is referred to as the isotropic coefficient as it remains invariant with rotation whereas $b^{(3)}$ and $c^{(3)}$ vary with ϕ and are called the anisotropic coefficients. For p-input and output polarization the observed intensity modulation upon azimuthal rotation, the rotational anisotropy, arises from the interference between these anisotropic and isotropic terms. The SH patterns can best be understood by considering how these two polarizations interfere, as illustrated in Fig. 2. In this simple example, both the isotropic and anisotropic polarizations are chosen to have the same magnitude. If the polarizations are in phase, as in Case 1, they will constructively (or destructively) interfere and there will be three "peaks" in the rotational spectrum. If they are out of phase and do not interfere, the rotational spectrum yields 6 "peaks" as shown in Case 2. Naturally, these are two extremes; in most cases the contributions are not completely in phase or out of phase. A fit to Eq. (18) yields the ratio $c^{(3)}/a^{(\infty)}$, which contains a magnitude and phase angle reflecting this interference under the experimental conditions. In general, not only the susceptibility elements but the Fresnel coefficients will influence this interference since Snell's Law for complex media requires not only a change in magnitude but a change in phase as the light field traverses the interface.[14] Rotational anisotropy measurements under these polarization conditions are very sensitive to relative changes in both magnitude and phase of either the isotropic or anisotropic contributions.

With a judicious choice of both the input and output polarizations, one can effectively isolate three of the four independent tensor elements for this surface symmetry. There are five such combinations polarizations that are of interest when probing a surface of C_{3v} symmetry with optical SHG.

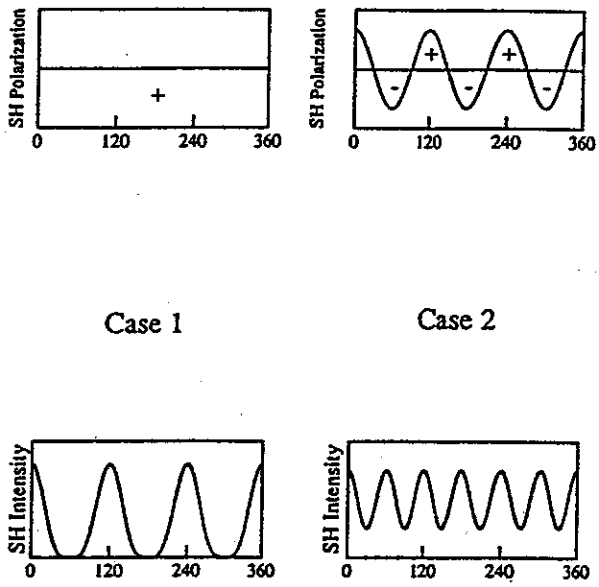

Fig. 2. Shown is the azimuthal dependence of the second harmonic polarization for the isotropic (top left) and anisotropic (top right) terms. Case 1 and 2 illustrate the resultant second harmonic intensity if the two terms constructively interfere or do not interfere, respectively.

For the dipolar response, they are the following:

$$I_{p,p}^{(2\omega)}(\phi) \propto \left| \begin{array}{c} F_z\chi_{zzz}f_zf_z + F_z\chi_{zxx}f_xf_x + F_x\chi_{xxz}f_zf_x \\ +F_x\chi_{xxx}f_xf_x\cos(3\phi) \end{array} \right|^2, \qquad (20)$$

$$I_{p,s}^{(2\omega)}(\phi) \propto \left|F_y\chi_{yxx}f_xf_x\sin(3\phi)\right|^2, \qquad (21)$$

$$I_{s,s}^{(2\omega)}(\phi) \propto \left|F_x\chi_{xxx}f_xf_x\sin(3\phi)\right|^2, \qquad (22)$$

$$I_{s,p}^{(2\omega)}(\phi) \propto \left|F_z\chi_{zyy}f_yf_y + F_x\chi_{xyy}f_yf_y\cos(3\phi)\right|^2, \qquad (23)$$

$$I_{m,s}^{(2\omega)}(\phi) \propto \left|F_y\chi_{yyz}f_zf_y + F_y\chi_{yxy}f_xf_y\sin(3\phi)\right|^2, \qquad (24)$$

where the intensity subscripts refer to the polarizations of the fundamental and SH light, f_i and F_i are the Fresnel coefficients of the fundamental and SH fields, and the χ_{ijk} represent the surface dipole susceptibility elements. In the case of Eq. (24), the subscripts m refers to mixed polarization

comprised of 50% p- and 50% s-polarization. These different polarization conditions allow isolation of the different source polarizations to the overall SH response from this interface and facilitate detailed studies of the sensitivity of SHG to both surface modification and changes in excitation wavelength.

Although rotational anisotropy measurements alone have been used to infer resonant behavior on metals, these can be misleading due to the number of tensor elements involved and because only relative phase and intensity information can be extracted. The selected polarization conditions shown above, at an azimuthal angle of $\phi \approx 30°$, are useful for separating these different contributions to probe their dispersion. For example, p-in and s-out polarization isolates the in-plane, or anisotropic, response contained in the coefficient $b^{(3)}$ (and $c^{(3)}$) arising from the susceptibility elements χ_{xxx} and ζ^Q (an electric quadrupolar element). At this azimuthal angle, p-in and p-out polarization isolates the $a^{(\infty)}$ term, which contains the surface dipolar terms χ_{zxx}, χ_{xzx}, and χ_{xxz} as well as possible contributions from higher order bulk susceptibility terms γ^M (a magnetic dipolar contribution) and ζ^Q (an electric quadrupolar contribution).

2.3. *Resonance Effects*

In centrosymmetric media such as fcc silver, SHG is forbidden under the electric dipole approximation in the bulk, but allowed at the metal surface where inversion symmetry is broken. Because of this broken centrosymmetry, the surface dipole susceptibility elements χ_{ijk} that describe this SHG process are particularly sensitive to the surface and it's associated electronic properties. The relationship between the dispersion of the tensor elements of $\chi^{(2)}$ and the electronic band structure can be described in single-particle excitation picture by the following equation,[11]

$$\chi^{(2)}_{ijk}(2\omega;\omega,\omega) = -Ne^3 \sum_{(a,b,c)} \frac{\langle c|r_i|a\rangle \langle a|r_j|b\rangle \langle b|r_k|c\rangle}{(2\hbar\omega - E_{ca} - i\hbar\gamma_{ca})(\hbar\omega - E_{ba} - i\hbar\gamma_{ba})}, \tag{25}$$

where r_i is the cartesian coordinate dipole operator, and, $|a\rangle$, $|b\rangle$, and $|c\rangle$ represent the initial, intermediate and upper state, respectively. It is clear from this expression that when either the fundamental or SH photon energy approaches the energy of an optical transition between two single particle states, χ_{ijk} may be resonantly enhanced and the resulting signal will differ

from the nonresonant case in both phase and intensity. The presence or absence of a resonance is further constrained by the matrix elements in the numerator, which are determined by the symmetry selection rules for coupling two single particle states with the optical field.

When probing the dispersion of the SH response from single crystal metal surfaces, the azimuthal-dependence of the response described above may be exploited to separate individual components of the overall surface response and to obtain information about the optical phase of the response. This will prove useful in identifying resonance behavior in the SH response from surfaces.

2.4. *The Electrochemical Interface and Second Harmonic Generation*

Since most of the studies to be described pertain to the metal/electrolyte interface, a brief description of the electrochemical double layer in necessary. Shown in Fig. 3 is a simple schematic of the metal/electrolyte interface, illustrating the different types of ion-metal electrode interactions. The whole region in which the charged species and oriented dipoles exist at this interface is referred to as the electrical double layer. One class of adsorption, sometimes referred to as nonspecific adsorption, arises from a combination of image forces (dipole–dipole) and London forces (induced dipole-induced dipole) as the hydrated ion approaches the electrode.[15] This plane corresponds to the center of mass of the hydrated ion in closest approach to the electrode surface and is called the outer Helmholtz plane (OHP) as shown in Fig. 3. The other type of electrolytic adsorption process is more chemical in nature in that the ion partially sheds its solvation shell and in an analogous manner defines the inner Helmholtz plane (IHP). In this case, the ion chemisorbs, or bonds ionically or covalently to the surface.

An electrode at which no faradaic process (charge transfer across the interface) can occur regardless of applied voltage is referred to as an ideal polarized electrode (IPE). For real systems, there may exist a range of applied potentials, the ideally polarizable region (IPR), in which an electrode (in a nonspecifically adsorbing electrolyte) behaves ideally polarizable. Within the IPR of such a system, since charge cannot cross the IPE interface, the charging behavior of the electrode–solution interface is analogous to that of a capacitor with a capacitance C:

$$C = q/V_{dc}\,, \tag{26}$$

where q is the charge stored on the capacitor plate and V_{dc} is the voltage across the capacitor. Whether the charge on the metal is positive or negative with respect to the solution depends on the potential applied to the metal. Furthermore, there exists an applied potential, the potential of zero charge (PZC), where there is no excess surface charge on the metal electrode. This potential is of interest as it represents the condition whereby the perturbation of the metal electrode surface is minimized. At the PZC, the electrode surface possesses the greatest chance to have the properties of the metal in the absence of the double layer—namely, that of a surface in vacuum.

When the electrode is biased away from the PZC, excess charge accumulates at the metal surface. Since metals screen efficiently, the excess charge on the metal is localized on the top atom layer of the surface; this charge is counterbalanced in the electrolyte by the ions in ~ 10 Å from the interface. Upon considering Eq. (25) it becomes clear that a voltage drop (~ 1 Volt) across this interface, which occurs on the order of ~ 10 Å, results in a DC field oriented perpendicular to the interface with a strength of 1V/10 Å, or 10^9V/m.

It is the large magnitude of this field that facilitates its coupling to the nonlinear polarization at the interface. In the first study of SHG from a solid/liquid interface, Lee[16] found the SH response from polycrystalline Ag and Si electrodes varied quadratically with the dc bias potential. They used the following expression to describe the additional third-order polarization induced by this dc field at this interface between isotropic media:

$$I^{(2\omega)}(\mathbf{E}_{dc}) \propto \left|P_0^{(2\omega)} + P_1^{(2\omega)}(\mathbf{E}_{dc})\right|^2 . \tag{27}$$

Here the total SH signal as a function of applied potential is written as a sum of a potential independent $P_0^{(2\omega)}$, which is the usual expression, and a potential-dependent part $P_1^{(2\omega)}$, which was described by the following:

$$P_1^{(2\omega)}(\mathbf{E}_{dc}) = \gamma \mathbf{E}_{dc}\left(\mathbf{E}(\omega) \bullet \mathbf{E}(\omega)\right) + \gamma \mathbf{E}(\omega)\left(\mathbf{E}_{dc} \bullet \mathbf{E}(\omega)\right)\,, \tag{28}$$

where $\mathbf{E}_{dc}$ is the static electric field oriented normal to the surface and γ, γ' are material constants describing the coupling to the static field. The SH response from the interface between isotropic media is described by a $\chi^{(2)}$ that contains only three independent tensor elements: χ_{zxx}, χ_{xzx},

and χ_{zzz}. This process can be viewed as a mixing of a static field that induces a polarization strictly oriented in the z direction (normal to the electrode surface) and the polarization induced by light waves.

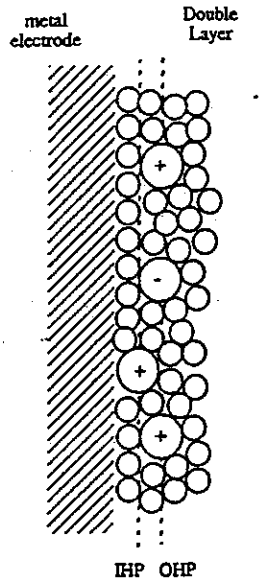

Fig. 3. A simple schematic of the metal/electrolyte interface, illustrating the different types of ion-metal interactions. The inner Helmholtz region (IHP) and outer helmholtz region (OHP) are denoted by dashed lines.

This additional polarization at the surface is the result of a mixing process that can be written as the following[17,18]

$$P_i^{(2\omega)}(\mathbf{E}_{l_{dc}}) = \chi_{ijkl}^{\prime(3)} \mathbf{E}_j(\omega)\mathbf{E}_k(\omega)\mathbf{E}_{l_{dc}} , \tag{29}$$

where $\chi^{\prime(3)}$ is distinct from the third-order term in Eq. (2) that describes the induced polarization at 3ω. Since both $\chi^{(2)}$ and $\chi^{\prime(3)}$ have the same symmetry constraints imposed by the electrode surface, the overall symmetry of the response remains unchanged and the net effect is that most tensor elements will be enhanced by the interfacial charging. It is important to note that in Eq. (28) the dc field-induced polarization perpendicular to the surface can only directly couple to either the fundamental or SH polarization normal to the surface. However, if both the fundamental and SH fields are in the plane of the surface ($i = x, y$), the full expression for the effective nonlinear polarization is the following:

$$P_{i,\text{eff}}^{(2)}(2\omega) = \vec{\chi}^{D} : E_i(\omega)E_i(\omega) - \nabla \cdot \left[\vec{\chi}^{Q} : E_i(\omega)E_i(\omega)\right] , \tag{30}$$

where in the second term the divergence results in contributions from both the quadrupolar tensor $\vec{\chi}^Q$ and the fundamental fields $E_i(\omega)$ but neither is surface sensitive in this case. Therefore, the only available mechanism for the charging of the interface to couple to these terms is through changes in the tensor $\vec{\chi}^D$.

3. Experimental Considerations

The optical schematic encompassing most of the SH experiments is shown in Fig. 4. For the optical measurements at 1064 nm and 532 nm excitation, the fundamental or second harmonic output from a 10 Hz Nd:YAG laser producing 10 ns pulses has traditionally been used although one can also employ other shorter pulsed higher repetition rate lasers. The 532 nm

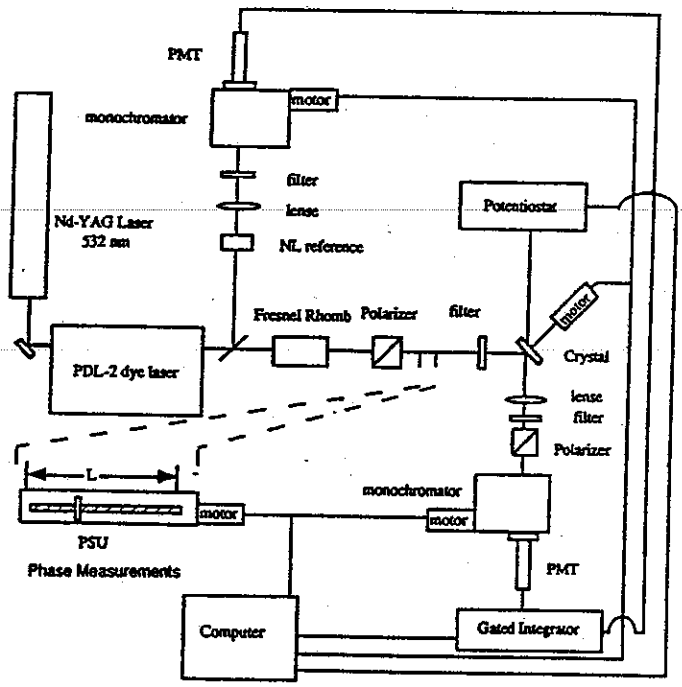

Fig. 4. Diagram of the optical second harmonic generation experiments showing the schematic for both the fixed frequency measurements and the wavelength scan measurements.

light can also be used to pump a tunable dye laser when spectroscopy measurements are desired. In some of the experiments to be described, the Nd:YAG laser also pumped an optical parametric oscillator which generates tunable IR light near 1.5 and 3.0 microns. High extinction coefficient

broadband polarizing beamsplitting cubes are used to select the polarization of the light striking the metal surface and of the SH generated at the surface. For the fixed frequency experiments, where power levels are kept near 2 mJ/(pulse-cm^2), it is not necessary to normalize for power. However, for the dye laser (dispersion) experiments, a reproducible reference channel is necessary to follow both the quadratic-dependence of the SH intensity upon the fundamental power and the ω^2-dependence of the SH intensity with changes in frequency, as shown in the following expression:

$$I(2\omega) = \frac{32\pi^2\omega^2\sec^2\theta_{2\omega}}{c^3\varepsilon(\omega)\sqrt{\varepsilon(2\omega)}}\left|E(2\omega)\chi^{(2)}_{s,\text{eff}} : E(\omega)E(\omega)\right|^2 I^2(\omega)\,, \qquad (30)$$

where $\theta_{2\omega}$ is the refracted angle of the SH beam from the surface. To do this, a portion of the incident light can be directed into a 1 mm long quartz cell containing a suspension of KDP powder in decahydronapthalene.[19] The transmitted SH light thus served as a reference to normalize for the quadratic dependence of SHG and to correct for intensity variations in the dye laser gain curve. Appropriate filters and a monochromator are used to separate the second harmonic signal (or reference) from the specularly reflected (or transmitted) fundamental light.

The relative phase of the SH signals can be measured by an interference technique,[20] where an additional wave at 2ω is generated by inserting a harmonic wave plate in the path of the incident beam prior to the sample (see Fig. 4). By changing the distance L between the quartz plate and the sample, an interference pattern is generated as a result of the small but non negligible dispersion in air. This is manifested as a phase lag in the SH generated from the quartz relative to the fundamental as both beams propagate toward the sample. The relative phase $\Delta\delta$ between the SH generated at the quartz plate and that of the sample depends on the change in distance between the quartz and the sample in the following manner[21]:

$$\Delta\delta = \left(\frac{2\omega}{c}\right)\Delta n \Delta L\,, \qquad (32)$$

where Δn represents the difference in the index of refraction of air at the fundamental (ω) and harmonic (2ω) frequencies and ΔL is the length the quartz plate is translated. For 1064 nm excitation, ΔL is of the order of 22 cm.

For the experiments conducted in vacuum, the light is coupled in and out of the chamber through appropriately placed windows.[22,23] For both the solution and ultrahigh vacuum (UHV) experiments, one uses Laue X-ray diffraction as a first-order check of the orientation and quality of the surface. One generally employs other conventional techniques for monitoring the quality and cleanliness of the surface including Auger and LEED. In many of the studies described below, the crystal is rotated azimuthally by 360° inside of the chamber. In our laboratory the crystal is mounted on a manipulator which is computer interfaced for control. The angle of incidence used is 31°. The surfaces are generally sputtered and annealed by standard methods.

For the electrochemical measurements to be described the surfaces are first mechanically polished and then electrochemically polished with appropriate solutions to remove the damage layer from the mechanical polishing. The electrochemical polishing and subsequent transfer of the crystal to the electrochemical cell are all done in an oxygen free environment to avoid oxide formation. All solutions are prepared from high-purity salts and Nanopure water and the electrolyte is continuously purged with oxygen free nitrogen throughout the electrochemical experiments to avoid oxide formation. The cell is constructed from Kel-F and has a rotating shaft which allows for the rotational anisotropy measurements.[17]

4. Summary of Experimental Results

4.1. *Ag(111), Ag(110) and Ag(100)*

The first studies of single crystal Ag surfaces which were performed in solution focused primarily on demonstrating that the SH response was from the silver single crystal surface and that this response was potential-dependent.[17,24–30] Several of these studies have been performed in solution with parallel UHV studies for comparison.[31–33] The focus of most of this work has been to understand the effect of the double layer on the geometric and electronic structure of Ag surfaces in solution. In the course of these experiments some very interesting issues have arisen calling into question theoretical efforts in this area which are based on a jellium approach to modeling the nonlinear optical response from metal surfaces. To clearly address these issues, the solution studies have been accompanied by parallel UHV studies with the results summarized below.

When an illuminated Ag(111) surface is rotated about its surface normal, the SH response observed in reflection is found to vary in a sinusoidal manner consistent with the 3m symmetry of the surface region. Figure 5(a) shows the results for Ag(111) under UHV conditions.[31] The 1064 nm incident beam is *p*-polarized with the *p*-polarized SH response monitored at 532 nm. As the surface is rotated azimuthally through 360°, the anisotropy in the SH response is clearly evident. To ensure that this anisotropy was not due to surface oxides or other contaminants, the surface was sputtered and analyzed by Auger. The annealed surface yielded a sharp LEED pattern characteristic of a well ordered (1×1) Ag(111) surface.

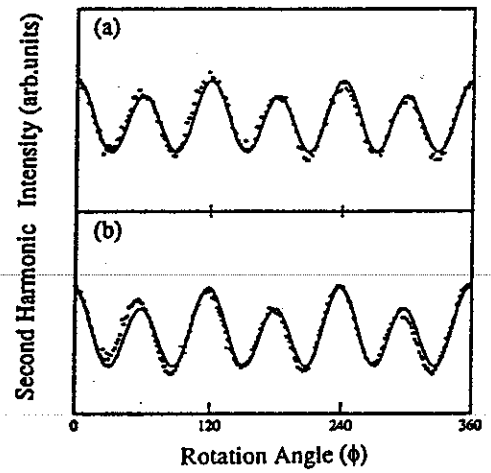

Fig. 5. The SH rotational anisotropy under 1064 nm excitation for p-input and p-output polarization from a Ag(111) surface (a) in UHV where $c^{(3)}/a^{(\infty)} = 1.0e^{i86^\circ}$, and (b) in 0.1 M $NaClO_4$ electrolyte biased at the PZC, −0.7 V vs Ag/AgCl;$c^{(3)}/a^{(\infty)} = 1.2e^{i85^\circ}$.

The observation of rotational anisotropy from Ag(111) in UHV demonstrates that the SH response is not purely free electron in nature as has been presumed for metals where neither ω nor 2ω are within the range of surface resonances. A similar conclusion was made in earlier[30,34–36] but verification in UHV was necessary to eliminate the possibility that water dipole-induced surface states or surface oxide contaminants could be an important factor in the observed anisotropy *in situ*. Studies of Koos *et al.* on Ag(111), Ag(110) and Ag(100) electrodes have shown that this anisotropic response from Ag at this wavelength originates primarily from the surface with only a minor contribution from the bulk.[37]

To attempt to understand the effect of the electrolyte and the applied

dc field on the surface properties, parallel solution and UHV studies were performed. For the electrochemical measurements the applied potential was restricted to be within the ideally polarizable region (IPR) in order to avoid faradaic electrochemical reactions which could alter the composition and morphology of the surface. An example of the cyclic voltammogram resulting from potential variation within this region is shown in Fig. 6 for Ag(111) in 0.1 M Na_2SO_4. For comparative purposes with the SH measurements in UHV, data was collected at the potential of zero charge (PZC) in order to minimize the effect of the dc electric field on the surface properties. Figure 5(b) shows the results for Ag(111) electrode biased at the PZC in a nonspecifically adsorbing 0.1 M Na_2SO_4 solution. The qualitative similarity between these two SH results is striking. The results for the two environments are also similar with the *s*-polarized output monitored.

A more quantitative comparison can be made by examining the fitting parameters for the two anisotropy patterns. Using Sipe's notation,[13] the

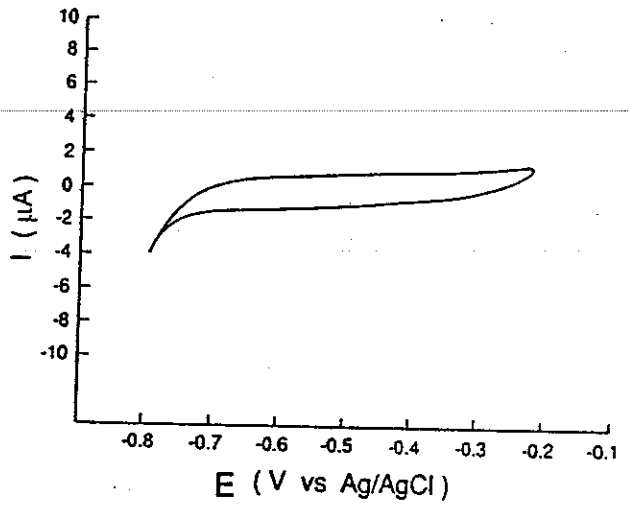

Fig. 6. Cyclic voltammogram of Ag(111) immersed in 0.01 M $HClO_4$ at pH = 2, scan rate of 20 mV/sec.

p-polarized SH response from a (111) surface excited by *p*-polarized input obeys the phenomenological expression previously discussed in Eq. (18). The fits to the data provide the following relative magnitudes and phase angles of the phenomenological constants $c^{(3)}$ and $a^{(\infty)}$ where

$$c^{(3)}/a^{(\infty)} = 1.0(\pm 0.1)e^{i86^\circ}, \tag{33}$$

$$c^{(3)}/a^{(\infty)} = 1.2(\pm 0.1)e^{i85^\circ} \tag{34}$$

for the UHV and PZC measurements, respectively. The results for the two environments are essentially identical within experimental uncertainty. This suggests that the possible alteration of the surface optical properties due to the presence of the water layer is negligible, as measured by the ratio $c^{(3)}/a^{(\infty)}$ and that the SH measurements in solution are a good approximation of the properties of the surface prepared and analyzed in UHV. These conclusions are consistent with the results of LEED UHV-transfer experiments performed by Hubbard and coworkers.[38]

Tests have been performed to demonstrate that this similarity is in fact real and is not merely due to the insensitivity of SHG to the surface properties. In the UHV experiments, when the surface is intentionally perturbed by dosing with K, a significant change in the overall SH response is observed which is mainly manifested in the $a^{(\infty)}$ term. Subsequent sputtering of the crystal to remove the K followed by annealing restores the original rotational anisotropy. Similar sensitivity to surface perturbation has been demonstrated in solution. With the growth of an oxide layer on the surface, the overall SH response is diminished. As the surface is electrochemically roughened, the anisotropy eventually disappears.[35] As will be discussed in more detail below, as the potential bias is varied beyond the ideal PZC conditions, these anisotropies vary from what is observed in UHV.

4.1.1. *Wavelength Dependent Studies of Ag(111)*

The bulk electronic structure of a material is reflected in the linear dielectric function. How the nonlinear response is related to this linear dielectric function of the material via the linear Fresnel coefficients has been the focus of theoretical efforts. The focus of the studies described in this section is to examine the sensitivity of SHG to electronic structure *in situ* and to test the correlation between the linear optical properties of the metal and the nonlinear response. The first studies to be described pertain to analysis of surface resonances whereas the second part examines the response under nonresonant conditions.

4.1.1.1. *Resonant Studies*

The linear optical properties of the noble metals silver, copper, and gold have been measured extensively and have been previously tabulated along with the optical constants of other materials.[39] The dielectric function for

a given material is defined by the following expression:

$$\varepsilon(\omega) = \varepsilon_1(\omega) + i\varepsilon_2(\omega) \tag{35}$$

where $\varepsilon_1(\omega)$ and $\varepsilon_2(\omega)$ denote the dispersive and absorptive components of the complex dielectric function ε and are related to the complex refractive index $N = n+ik$ by $\varepsilon = N^2$. The dielectric function is the preferred method of expressing the relationship between the optical properties and the band structure of solids because the absorptive part of the dielectric function does not depend on the refractive index.[40] For silver, at low energies up to 3.5 eV the real, or dispersive component of the dielectric function $\varepsilon_1(\omega)$ dominates, but near 4 eV the onset of absorption by both the *d*-bands and the *sp*-bands is reflected in the abrupt rise in $\varepsilon_2(\omega)$. Since the electronic properties as manifest through the linear optical properties show structure in this spectral region, it seems reasonable to expect the nonlinear optical properties to exhibit a similar coupling to the electronic structure of silver.

Several studies have examined the wavelength-dependence of the rotational anisotropy in the resonant SH response for Ag(111) in electrolyte solutions.[32,41,42] These studies include both solution and comparative UHV studies and examine the nonlinear response over a broad spectral range in the visible region where the SH photon energy is sufficiently energetic to couple to the onset of electronic structure. Figure 7(a–e) shows the rotational anisotropy for *p*-input and *p*-output polarizations from a clean Ag(111) crystal biased at the PZC in 0.1 M $NaClO_4$ electrolyte at a series of excitation wavelengths. The PZC bias potential was chosen to minimize the effect of the dc field across the electrochemical interface.[9] At each excitation wavelength the data can be fitted well by the functional form given in Eq. (18) and the fitted parameters for each excitation wavelength are given in Table 1. One observes a variation in both the amplitude and the phase of the response with incident wavelength with the most dramatic changes occurring in the spectral region near $\lambda_{SH} \approx 320$ nm where the sharp increase in $\varepsilon_2(\omega)$ is seen. As the incident photon energy increases, the progressive change in the anisotropies is best described by the change in the phase angle of $c^{(3)}/a^{(\infty)}$, the difference in phase between the in-plane and out-of-plane response. This is the first study to demonstrate the sensitivity of these SH anisotropy measurements to wavelength.[31,32] The overall change in pattern and associated phase angle has been attributed to increased coupling of the harmonic field to electronic transitions near 3.9 eV. When comparative

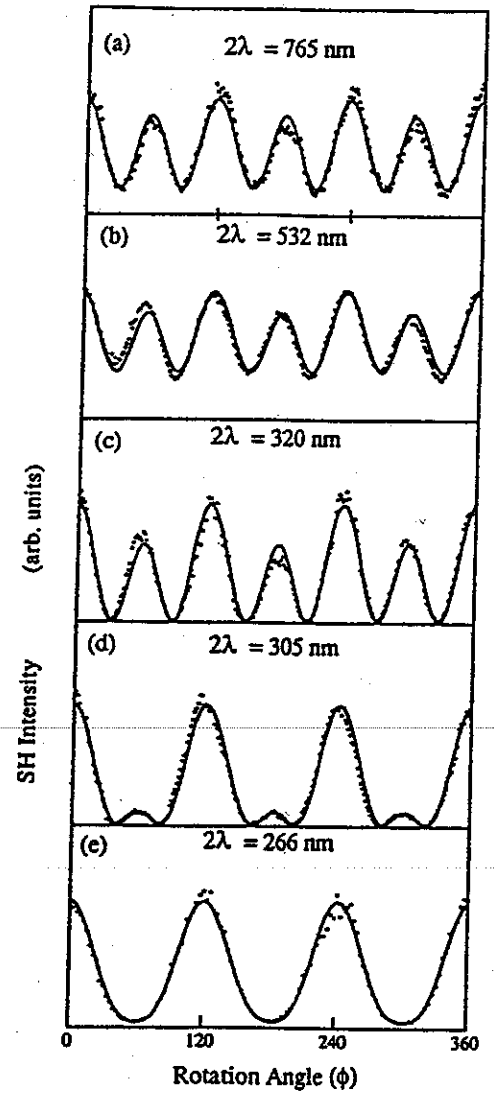

Fig. 7. The SH rotational anisotropy from a Ag(111) surface in 0.1 M $NaClO_4$ electrolyte biased at the PZC with p-input and p-output polarization at the following harmonic wavelengths: (a) λ_{SH} = 765 nm, (b) λ_{SH} = 532 nm, (c) λ_{SH} = 320 nm, (d) λ_{SH} = 305 nm, and (e) λ_{SH} = 266 nm. From Ref. 41.

studies were performed on Ag(111) in a UHV environment, the SH response from the surfaces in the two environments were found to be nearly identical. As demonstrated by the fits to the data tabulated in Table 1, the amplitude and phase of the $c^{(3)}/a$ ratio is remarkably similar for all wavelengths. This is not however found to be the case when the electrode surface is

Table 1. Wavelength Dependence of the Rotational Anisotropy from Ag(111) in UHV and in Solution, Held at the PZC. Fitting Parameters from Eq. (16).

SH photon energy, eV	λ_{exc} (nm)	$c^{(3)}/a^{(\infty)}$ Solution	UHV
1.62	1530	$1.7e^{i85°}$	
2.33	1064	$1.2e^{i86°}$	$1.2e^{i85°}$
3.875	640	$5.4e^{i57°}$	$3.95e^{i81°}$
4.065	610	$1.85e^{i18°}$	$1.74e^{i42°}$
4.66	532	0.6	0.7

biased to either side of the PZC. For excitation wavelengths near $\lambda_{SH} \approx$ 320 nm, strong differences are observed between the solution and the UHV data.[41] From rotational anisotropy measurements made at fixed incident frequencies near the peak (λ_{SH} = 320 nm) the potential-dependence is even more striking. For these (p,p) measurements, large changes in the relative phase angle of the ratio $c^{(3)}/a^{(\infty)}$ is observed which leads to large variations in the patterns. Figure 8 provides an example of this type of data in which the relative phase angle varies from 120° to 57° to 41° as the surface is biased at −0.2V, −0.7V (PZC) and −1.2 V respectively. Potential-dependence is also seen in the p-in and s-out data in which χ_{xxx} is the only dipolar term accessed. Since the Thomas–Fermi screening length in a metal is of the order of one atomic layer, the applied potential is rapidly screened at the surface. Thus potential-dependence in the SH response must originate from the surface region. The authors conclude that the potential-dependence in this region is due to potential-induced changes in the surface electronic structure.[32,41]

Later studies have analyzed the dispersion in the SH response as the surface examined in both solution and in UHV is held at a fixed rotational angle.[32,33] Figure 9(a) shows the explicit wavelength-dependence of the normalized SH intensity from Ag(111) in UHV for p-input and s-output (p,s) polarization from λ_{SH} = 307 nm to λ_{SH} = 375 nm. The normalized intensity shows a sharp peak at λ_{SH} = 325 nm (3.82 eV), with a FWHM of 100 meV. The solid line in Fig. 9(a) represents a least squares fit to the data for a fitting function discussed in the work. Figure 9(b) shows the

corresponding measurement of the normalized SH intensity from Ag(111) in UHV for p-in and p-out (p,p) polarization, with the curve as a guide to the eye. No peak is observed here and the intensity at the lower energy appears relatively dispersionless. The significantly lower overall intensity

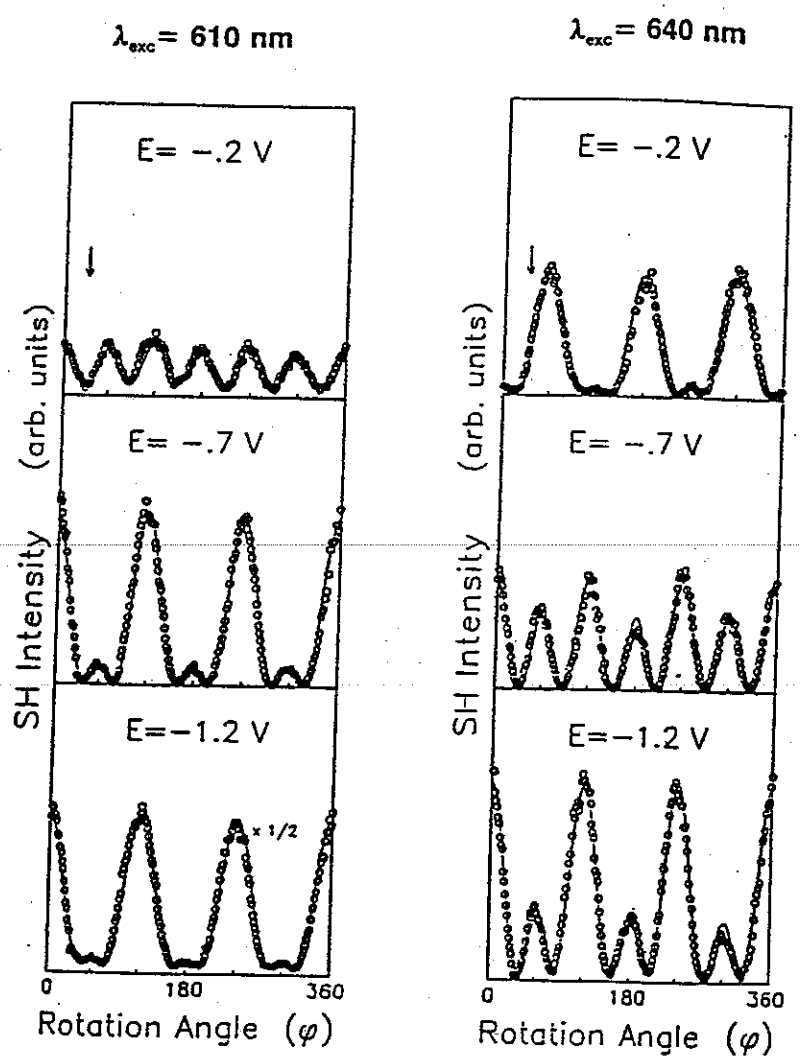

Fig. 8. SH intensity as a function of azimuthal rotation for Ag(111) in 0.1 M $NaClO_4$ under p-polarized excitation at the wavelengths and electrode potentials indicated. All electrode potentials reported versus Ag/AgCl reference. The open circles are the p-polarized SH experimental data and the solid lines are fits to Eq. (1). Fitting parameters for 610 nm data at $E = -0.2$ V, $E = -0.7$ V, and $E = -1.2$ V are $c^{(3)}/a^{(\infty)} = 1.8e^{i86^\circ}$, $c^{(3)}/a^{(\infty)} = 1.85e^{i18^\circ}$, and $c^{(3)}/a^{(\infty)} = 1.1e^{i30^\circ}$, respectively. Fitting parameters for the 640 nm data at $E = -0.2$ V, $E = -0.7$ V, and $E = -1.2$ V are $c^{(3)}/a^{(\infty)} = 1.24e^{i120^\circ}$, $c^{(3)}/a^{(\infty)} = 5.4e^{i57^\circ}$, and $c^{(3)}/a^{(\infty)} = 2.4e^{i41^\circ}$, respectively. From Ref. 41.

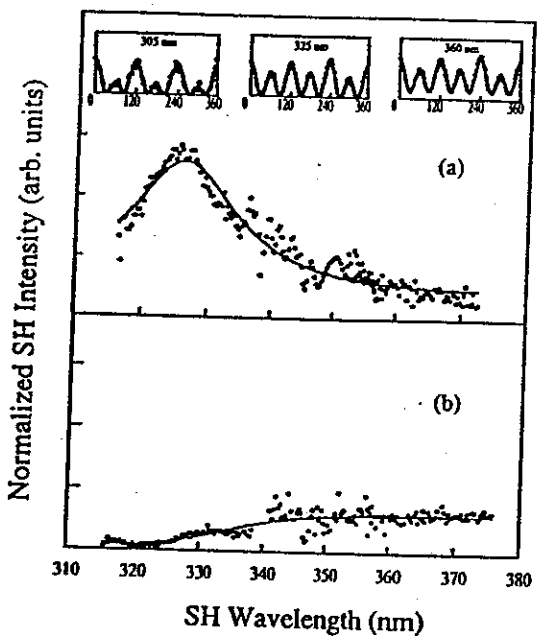

Fig. 9. Wavelength-dependence in the normalized SH response from Ag(111) ($\phi = 30°$) in UHVwith p-input polarization and (a) s-output polarization; (b) p-output polarization. The inserts represent the anisotropies measured for p,p-polarization conditions for various wavelengths within the scanned region. The fitting parameters for these anisotropies are $c^{(3)}/a^{(\infty)}$: (λ_{SH} = 305 nm) $1.74e^{i42°}$; (λ_{SH} = 325 nm) $3.954e^{i81°}$; (λ_{SH} = 360 nm) $2.16e^{i86°}$. From Ref. 33.

and different spectral-dependence of Fig. 9(b) relative to Fig. 9(a) suggests that the susceptibility elements that contribute to this response are probing different surface features than the χ_{xxx} dipolar element that is monitored in Fig. 9(a). The dispersion seen in the two wavelength scans of Fig. 9 are entirely consistent with anisotropy data at discrete wavelengths in this wavelength region, three of which are shown as inserts in Fig. 9(a).

For the parallel studies in solution, the experiments were conducted in 0.1 M $NaClO_4$ electrolyte since the ClO_{4-} ion is known to nonspecifically adsorb on silver.[43] Figures 10(a–c) show the normalized SH intensity from Ag(111) at three applied potentials for p-in and s-out (p,s) polarization from λ_{SH} = 307 nm to λ_{SH} = 375 nm. Figures 10(d–f) represent the corresponding (p,p) data. At the PZC, the solution data is very similar to the UHV data for both (p,p) and (p,s) polarizations. (Compare Fig. 10(b) and (e) with Fig. 9(a) and (b), respectively). This remarkable similarity in the two sets of data in the different environments implies that at the PZC,

the peak observed in UHV is not strongly perturbed by the presence of the electrolyte as was also the case for the rotational anisotropy plots described earlier. This similarity breaks down when the applied bias is held away from the PZC and a dc field develops across the metal/electrolyte interface. For (p,p) polarization in which the out-of-plane (isotropic) response is sampled (Fig. 10(e,f)) the nonresonant region ($\lambda_{SH} \geq 360$ nm) shows the strongest potential-dependence. These nonresonant results are entirely consistent with previous studies examining the potential-dependence using 1064 nm incident light. Quite interestingly, when experiments are performed which isolate the potential-dependence of the respective tensor elements involved in the isotropic response, χ_{xzx} is found to increase dramatically with positive charging.[33] Previous theoretical treatments have assumed that only χ_{zzz} is important.[44,45] Of equal importance are the potential-dependent

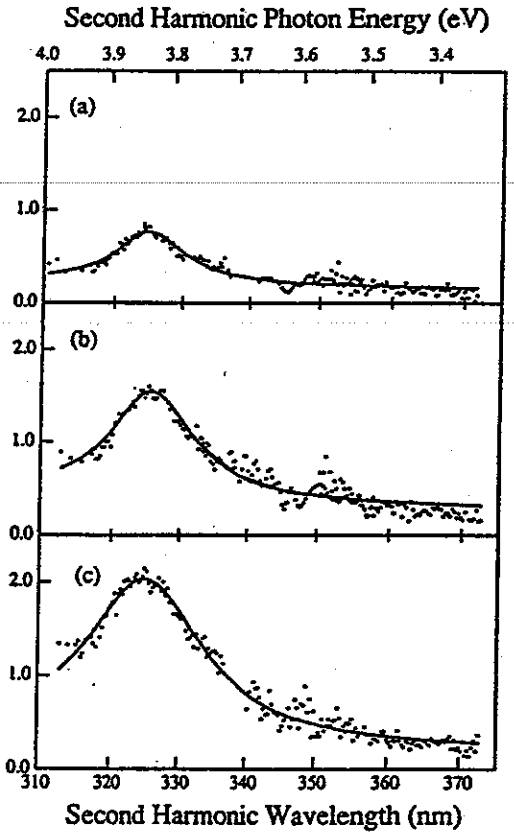

Fig. 10. Wavelength-dependence of the normalized SH intensity from Ag(111) ($\phi = 30°$) in 0.1 M $NaClO_4$ for (p,s)-polarization (a–c) and (p,p)-polarization (d–f). The potential was held at a positive bias, −0.2 V vs. Ag/AgCl for (a) and (d); near the PZC at −0.7 V for (b) and (e); at a negative bias at −1.2 V for (c) and (f). From Ref. 33.

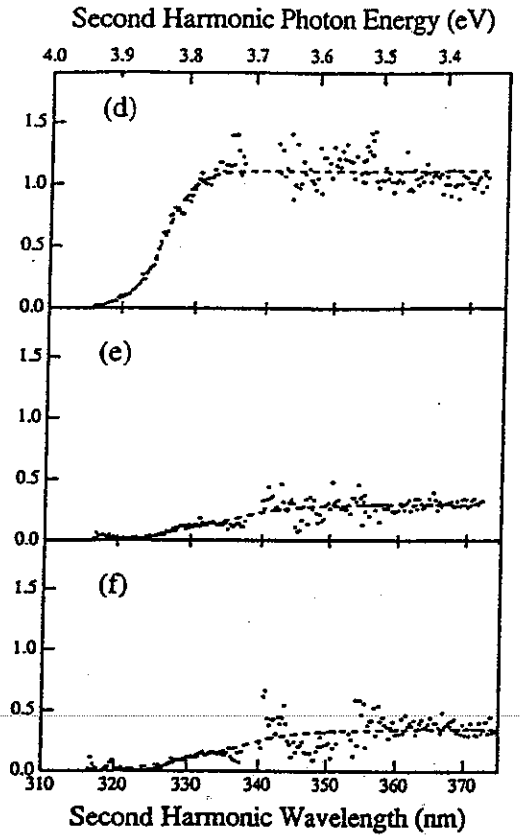

Fig. 10. (*Continued*)

results for (p, s) polarization since in these experiments the only dipolar term accessed is the in-plane χ_{xxx}. Biasing away from the PZC causes a variation in the intensity. The fact that such a strong potential-dependence of the peak is observed implies that the peak has significant contributions from the surface. Currently, no simple mechanism exists to account for the coupling of the applied field (in the z direction) to the in-plane χ_{xxx} susceptibility, as the tangential component of the electric field is continuous across the interface. The most plausible explanation for the observed charging behavior under these polarization conditions is potential induced changes in the surface electronic properties.

One has the advantage in electrochemical studies of being able to alter the surface potential so as to distinguish contributions from bulk electronic structure vs surface electronic structure. The potential-dependent behavior would suggest that surface electronic properties are playing a role in the

observation of a sharp peak at $\lambda_{SH} = 325$ nm. The most likely electronic transition in this region consistent with the measurements is a two photon optical transition from the occupied crystal induced surface state (A) to the unoccupied bulk band edge[33] based largely on the potential dependent studies. In the surface region where the applied potential is screened, the unoccupied bulk band edge and the surface state A will have a similar spatial profile and thus should energetically shift by a similar amount with applied potential. Surface state A is a plausible initial state for a resonant transition since it is spatially localized to the surface. Since it lies very close to the Fermi level, its energetic position relative to the bulk states and its occupation should be sensitive to an applied potential. In a manner analogous to the work function, the electrochemical potential will increase as the metal is charged positively because more work must be done to extract electrons from the Fermi level. Thus the bulk bands in the metal will be shifted to higher binding energy (relative to E_{vac}) under conditions of positive charging, but surface localized bands or states will shift less and move to a lower binding energy relative to the bulk bands as they experience some fraction of the applied potential. For state A, positive charging will lead to depopulation of the state as its energy is shifted above the electrochemical potential. For negative charging, state A will shift further below the electrochemical potential and increase in occupation. This is consistent with the intensity changes that are observed, assuming that any energetic shift is small relative to the peak width. At positive potentials, Fig. 10(b), the peak intensity drops, consistent with the depopulation of A. For negative charging, the reverse would be expected and is observed in Fig. 10(c).

In recent nonlinear electroreflectance measurements, Furtak *et al.*[46] examined the isotropic (p,p) SH response from Ag(111) over a range of SH photon energies from 2.8 eV to 4.46 eV, normalizing at each wavelength the potential-dependent SH response with the magnitude of the SH response observed at the PZC. In qualitative agreement with the results of Figs. 10 under nonresonant conditions, they found for positive charging that the SH response behaved in a manner consistent with the SH studies from polycrystalline silver,[18] where the SH response was modeled with local-density functional theory for jellium. However, under negative charging, Furtak *et al.* attributed a spectral feature near 3.4 eV to the above mentioned A-I transition (coupling to χ_{zzz}) and invoked the arguments of Schneider

et al.[47] to rationalize the appearance of the feature only under negative charging.

As noted in the work of Bradley *et al.*,[33] in addition to a surface electronic structure contribution, one must also consider that the peak in the SH spectra near 3.85 eV could be a simple result of the bulk dielectric properties of the metal. Since the dielectric constant of silver has structure in the spectral region near 3.8 eV, only the Fresnel coefficient for the radiated SH light, F_y, and not the Fresnel coefficient at the fundamental wavelength, f_x, will reflect this structure. Although calculated plots of the dispersion of F_s, F_k and F_z, exhibit structure near 3.8 eV due to the interband transitions of Ag, there are significant differences between the experimental observations and the calculations suggesting the surface electronic structure is a contributing factor.[33] Furthermore, the strongest evidence that electronic structure plays a role is that the Fresnel model cannot successfully describe this potential-dependence since it treats the surface as a boundary condition and only treats the fields in the bulk of the material. One might argue that as the potential is varied, the surface electronic density is modified which changes the screening of the intraband transitions at the surface. Consistent with what is experimentally observed, this would lead to an alteration of the intensity of the peak without perturbing the energy of the peak which is cominated by the Fresnel factor. However, the weakness in this argument is that at longer wavelengths no such charging in the in-plane response using p, s-polarization has been observed.[41] Nevertheless, the Fresnel factors must play a role to some degree.[48,49]

The observations described above raise an important issue regarding the use of rotational anisotropy plots to determine the geometric structure of a surface, particularly when the measurements are made at a single wavelength under (p,p) polarization conditions. If relative changes in phase are not considered, one might infer that the potential induced changes in the anisotropy patterns represent a potential induced reconstruction. Likewise, changes in rotational anisotropy upon adsorption of molecules might be attributed to the geometric orientation of the adsorbate at particular sites on the surface. Although both conclusions are likely valid under nonresonant conditions, at resonant or near resonant conditions, changes in phase which could accompany potential or adsorbate-induced changes in the electronic properties of the surface must be considered. It is therefore prudent to perform such measurements for at least several wavelengths before

drawing conclusions of changes in geometric structure as opposed to electronic structure based on rotational anisotropy data alone. Furthermore, measuring changes in geometric structure that effect changes in the overall surface symmetry demand appropriate choice of polarizations to unambiguously identify such symmetry changes.

Recently, Tang *et al.*[50] invoked a potential-induced surface reconstruction (from C_{3v} to C_3 symmetry) of Ag(111) as the source of changes in (p,p) rotational anisotropies in the spectral region near $\lambda_{SH} = 320$ nm. A potential-dependence was previously observed in the rotational anisotropies from Ag(111)[41] but these effects were described in terms of a changes in the relative phase angle since no evidence of such changes in symmetry were observed for any input and output polarizations. What is necessary to confirm such reconstruction is to observe it with (p,s) polarization where an isotropic term would add to an otherwise purely anisotropic response under C_{3v} symmetry.

4.1.1.2. *Nonresonant Studies*

If one is attempting to understand SHG from metal surfaces, the less complicated scenario is one in which resonance effects can be neglected. As noted earlier, under 1064 nm excitation Ag(111) exhibits strong rotational anisotropy where surface and bulk resonances should be a minor factor and cannot be used to justify the existence of the anisotropy. Such an experimental observation calls into question the use of jellium models to describe the SH response. Suggestions that this anisotropy is due to a quadrupolar contribution[51] are inconsistent with experimental measurements as are the suggestions that the anisotropy is due to surface oxides or steps on the surface.

The experimental studies by Wong *et al.*[52,53] have focused explicitly at this "long wavelength limit" in an attempt to understand both the magnitude and phase of the SH response. The experiments have examined Ag(111) and Au(111) in D_2O solutions using the 1.5 μm output from a Nd:YAG pumped optical parametric oscillator (OPO). The relative phase and absolute intensity of the response at this nonresonant wavelength are compared with the response with excitation at 1.064 mm and 0.532 mm (resonant). These results are then correlated with the dielectric properties of Ag and Au metal as one approaches nonresonant conditions. They find that as the long wavelength limit is approached, the absolute SH intensity

for both metals diminishes and converges to a small finite value. Their results for both Ag(111) and Au(111) are shown in Fig. 11. This convergence is consistent with the work of Georgiadis *et al.*[41] and Bradley *et al.*[33] for the resonance studies and the data shown in Table 1. Experimentally determined values for the contributing susceptibility tensors at the three wavlengths are reported. Cu(111) was also studied,[23,54] but due to the persistence of surface oxides when this electrode is in an electrolyte solution, the intensity and phase angle from the oxide free surface is not possible to obtain. They conclude that for Ag(111) and Au(111) the persistence of anisotropy under nonresonant conditions indicates that the rotational anisotropy in the SH response arises from an anisotropy in the electron plasma and does not involve interband transitions.

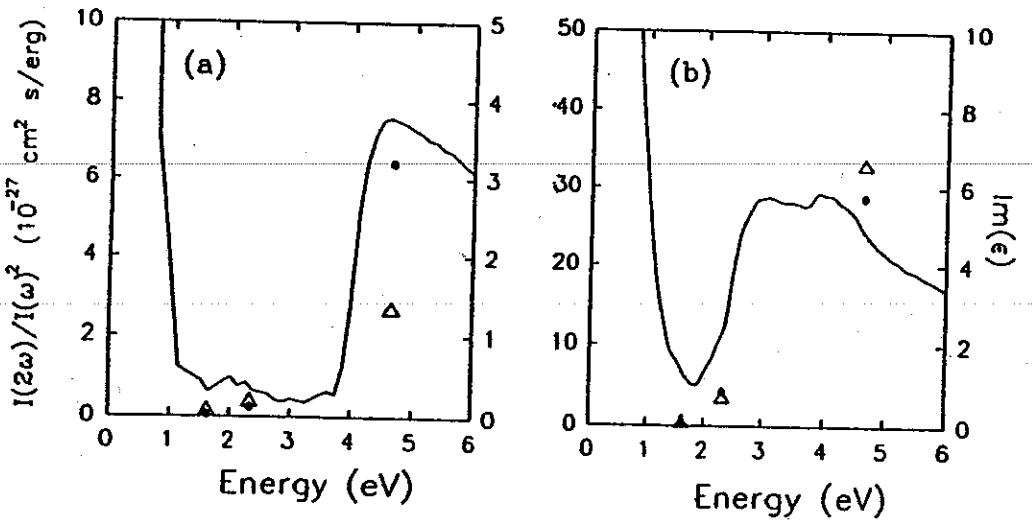

Fig. 11. Absolute SH intensity measurements with p-polarized input light as a function of SH photon energy, filled circles represent isotropic intensity, open triangles represent the anisotropic intensity, solid lines represent the imaginary part of the dielectric constant for metals, (a) Ag(111) and (b) Au(111). From Ref. 51.

One particular focus of the work is understanding the wavelength-dependence of the relative phase between the anisotropic and isotropic response and its behavior at the long wavelength limit. The phase data was derived from rotational anisotropy measurements similar to those described above. For both Ag(111) and Au(111) the phase angle varies from 0° under resonant conditions to $\pi/2$ at the long wavelength limit. They show that this convergence to $\pi/2$ at the long wavelength limit can be described in

terms of the phase difference between the in-plane and out-of-plane Fresnel factors for the fundamental and SH fields under nonresonant conditions. For the isotropic portion of the p-in and p-out response there are three surface contributions (χ_{zzz}, χ_{zxx} and χ_{xzx}) and their corresponding Fresnel factors. The anisotropic response is due only to the surface contribution of χ_{xxx} with appropriate Fresnel factors. It is not easy to determine how each Fresnel factor contributes to the phase difference between the isotropic and anisotropic response in the p-in and p-out experiment. However, by judicious choice of input and output polarization each contribution to the overall response can be isolated and the phase difference between the in-plane and out-plane Fresnel factors can be determined based on the common assumption that the susceptibility tensor elements become real under nonresonant conditions. Figure 12 shows the wavelength-dependence on the phase difference of the SH output Fresnel factor ($\delta_{2\omega} = \arg(Fz/Fx)$). The

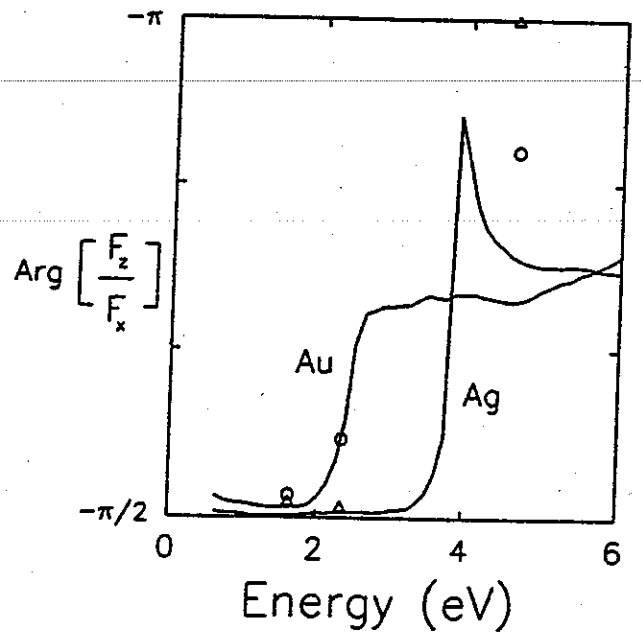

Fig. 12. The phase difference between the in-plane and out-of-plane Fresnel coefficients for the SH fields vs. SH photon energy. The triangles and circles represent the experimental values for the (a) Ag and (b) Au. From Ref. 51.

solid lines represent the calculation of the phase difference of the output Fresnel factors using the classical Fresnel model for silver and gold and the triangles and circles represent the experimental values for Ag and Au

respectively. Both the experimental results and the calculations show a convergence in the phase difference between the in-plane and out-plane Fresnel in the long wavelength limit of $\pi/2$. This phase difference can simply be viewed as a consequence of the delayed response of the electron between the in-plane and out-of-plane motion, which arises due to the boundary conditions imposed on the out-of-plane motion at the surface. This phase difference remains nearly constant until the value rises very abruptly at the onset of the interband transition. Whereas there is good agreement between experiment and theory for the long wavelength region, a clear deviation between experiment and theory is evident as resonant conditions are approached. This is to be expected since under resonant conditions it is difficult to predict the SH response from the metal as there are more variables to consider such as contributions from core-electrons, surface states and band transitions.

4.1.2. *Underpotential Deposition of Metallic Overlayers*

The SH response from single crystal electrode surfaces during underpotential deposition of metallic overlayers has been the focus of several studies. Underpotential deposition (UPD) is means by which controlled amounts of foreign metals can be deposited on electrode surfaces.[55] In studies to be described, several different metals have been underpotentially deposited on Ag(111) to determine if SHG can provide any information about the structural and electronic properties of the deposited overlayers. Koos *et al.*[17] examined the deposition of Pb and Tl on Ag(111) and Ag(110) using 1064 nm light. For a monolayer of Pb deposited on Ag(111), the interfacial region retains 3m symmetry for *p*-in and *p*-out although the ratio $c^{(3)}/a^{(\infty)}$ (Eq. 18) has undergone a phase shift of approximately $\pi/2$ relative to the native surface. The authors attribute this change in phase upon deposition to an optical resonance between 2ω and electronic states of the Ag/Pb interface. Thallium deposition on Ag(111) occurs up to a coverage of 2 ML and proceeds as a four step process. The SH response is clearly sensitive to each stage of the deposition and shows that the interfacial region retains its 3-fold symmetry throughout the deposition. Although there is little change in the overall intensity during the first three adsorption stages, a significant change in phase between the isotropic and anisotropic response is observed. At $\Theta = 2$ ML, a significant enhancement in intensity is observed. The authors attribute the large changes in the isotropic and anisotropic

contributions for $0 < \Theta < 1$ to the increased localization of electrons as the electronegative thallium atoms bond to the silver surface. For higher coverages, the authors attribute the increased signal to a resonance between either ω and 2ω with eigenstates in the overlayer which beyond one monolayer, approaches three dimensional bulk thallium structure. UPD of Tl on Ag(110) has also been examined.

Miragliotta and Furtak examined thallium deposition on Ag(111) using a continuous wave Nd:YAG laser.[56,57] Even though they were unable to observe anisotropy from the bare surface for this and a related study of the UPD of Zn and Cd on Ag(111) (Ref. 58), sensitivity to the deposition in all cases is evident. For thallium deposition, a $3m$ rotational symmetry is observed and is enhanced at 2 ML. By using a thin-layer cell, they were able to extend the deposition in a controlled manner to up to 4.1 monolayers. They propose that Tl grows with a coincidence lattice that is (6×6)-25 for all coverages. Significant to this and the previous analysis was the report of reflectivity measurements during deposition. A peak at 1.5 eV was observed upon formation of 1 ML of thallium on the surface. For the UPD of Cd and Zn on Ag(111), both metal adsorbates were found to produce significant increases in the SH response upon adsorption.[58] For Zn, where the symmetry of the SH pattern is of C_{3v} initially, the symmetry is found to change to twofold with further coverage. For Cd, they have reported resonant SHG from Cd as the monolayer is formed in a three-step process. Each step is presumed to be associated with one-third of a monolayer having $(\sqrt{3} \times \sqrt{3})$R30° symmetry. The overlayer is assumed to be epitaxial and buckled below two monolayers. Above two monolayers the entire overlayer appears to become incommensurate and closely packed.

4.1.3. *Stepped Crystal Surfaces*

Another related study on Ag(111) in electrolyte solution has been one which has investigated the role of steps and terraces on the SH response.[59] The results have important consequences for studies of surface reconstruction and for related studies in which one attempts to understand the importance and sometimes dominating role of steps and defects in surface electrochemistry. The studies involve rotational anisotropy measurements on a surface with a very high density of steps, a Ag(211) oriented crystal [19°28′ from the (111) surface], a vicinal surface which was cut with an offset of 4o towards direction and a flat Ag(111) surface. In such electrochemical

measurements one has the important advantage over UHV studies of readily and reversibly being able to apply this static field to the surface to either probe explicitly the surface response or to deposit foreign metals on the surface.

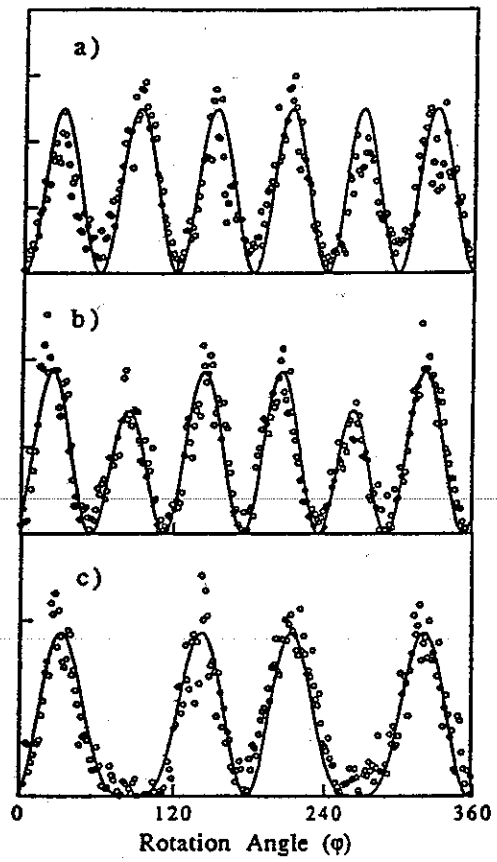

Fig. 13. SHG intensity from Ag electrodes at an applied potential of −0.5 V as a function of azimuthal angle for *s*-polarized SHG and *s*-polarized pump beam. Shown are measurements on (a) the flat Ag(111) surface, (b) the vicinal Ag(111) surface, and (c) the Ag(211) surface. From Ref. 57.

Shown in Fig. 13 are the rotational anisotropies obtained under s/s polarization conditions from the three surfaces in 0.1 M $NaClO_4$ electrolyte with an applied potential of −0.5 V vs SCE. Figure 13(a) shows the rotational anisotropy of Ag(111) [Ref. 24] which is similar to previous work. The data reflects the C_{3v} symmetry of this surface and is in excellent agreement with Eqs. (21) and (22). Figure 13(b) shows the rotational anisotropy of a surface vicinal to the Ag(111) ($\theta = 4°$), which in the case of only

monoatomic steps, corresponds to a notation introduced by Lang *et al.*[25] of 14(111) × (100). In Fig. 2(c) the rotational anisotropy of the SH signal of a crystal with a nominal (211) orientation is shown. This is highly stepped surface with a Land notation of 3(111) × (100). The data from the stepped surfaces in Fig. 13(b) and 13(c) clearly deviate from the pattern expected for a C_{3v} symmetry and can be explained by an additional onefold contribution, C_s, to the SHG superimposed onto the threefold contribution of the terraces. The only mirror plane preserved for the stepped surfaces is at $\varphi = 0°$. The existence of this mirror plane is evident in all rotational anisotropies of Fig. 13, since the intensity of 0° and 180° is zero. Their results show that the existence of a pseudo mirror plane at the steps has a stronger influence on the SH rotational anisotropies than the enhancement due to a stronger asymmetry at the in-plane termination of the crystal lattice. This suggests that the interpretation of the SH response requires consideration of the overall surface structure instead of just local components such as the step sites. Similar to the SH pattern from semiconductor surfaces[10] the signal from stepped metal surfaces exhibits a strong influence of the steps under nonresonant conditions. The underpotential deposition of lead on these surfaces was also examined. The nature of the adsorption processes in the Ag(111)/Pb^{2+} system enabled them to distinguish the changes in the SH response during adsorption at different geometric sites. It was also found that adsorption at defect sites exhibit a stronger influence on the SH intensity than adsorption on terraces, indicating that most of the contributions from the steps (and other defect sites) vanish by interference on the flat Ag(111) surface.

4.2. *Au(111), Au(110) and Au(100)*

Gold is not as reactive to oxygen as silver and copper but shows a stronger drive towards surface reconstruction than the other two. Because of the inert nature of gold, the IPR is also larger than Ag and Cu. For these combination of reasons, Au single crystal electrode surfaces have been the focus of much study and discussion in recent years.

4.2.1. *Examination of the Source of the SH Response*

The first study which reported rotational anisotropy from a gold electrode surface was performed on Au(111) using a 1064 nm incident beam.[60] This

work has recently been expanded in which Au(111) has been studied at several wavelengths.[22,53] Figure 14 shows the *p*-polarized SH response from Au(111) in $HClO_4$ using *p*-polarized excitation at 1530 nm, 1064 nm and 532 nm. The results are consistent with a surface of 3m symmetry and can be fitted well with the theoretical expressions of Eq. 18. There is a clear wavelength-dependence in the response as manifested in the fits to the data. These scans were taken at +0.8 V, positive of the PZC which occurs at 0.23 V (vs. SCE) in ClO_4- media. Identical scans performed in UHV for 1064 nm and 532 nm excitation show that the response in solution is nearly identical to that measured in UHV.[31] As with Ag(111), the phase angle between the in-plane and out-of-plane response ($c^{(3)}/a^{(\infty)}$) is found to vary from 0° to near 90° with decreasing incident photon energy. The authors attribute this variation in the anisotropy and corresponding change in magnitude and relative phase of the in-plane and out-of plane response to resonant coupling to electronic structure as the energy is increased. Absolute intensity measurements of the isotropic and anisotropic response from Au(111) at the three wavelengths were performed with the results provided in Fig. 11(b). For comparison, the imaginary part of the dielectric function is also plotted. For gold, the *d*-bands are near 2.0 eV, close to the 2.3 eV SH field. As with Ag(111) there is a strong drop in intensity as nonresonant conditions are approached. The convergence of the relative phase shift as nonresonant conditions are approached can, as with Ag(111), be described in terms of the linear Fresnel coefficients (Fig. 12). For resonant conditions, the fit is not as good.

Koos and Richmond[9] have examined the SH rotational anisotropy from Au(111) both under faradaic and nonfaradaic conditions using 1064 nm excitation. The studies were conducted on electropolished and flame annealed substrates. In the double layer charging region, a strong potential-dependence in the isotropic terms, and particularly χ_{zzz} is observed. They find that the simple surface charge density model is inadequate for describing the potential-dependent behavior for perchlorate and sulfate containing electrolytes, similar to what was found for Au evaporated films.[18] Their studies have also examined oxidation of Au(111) in both electrolytes. Oxide formation of Au is presumed to be a multistep process with one of the controlling steps being a place-exchange process involving the turn-over of the OH-Au dipoles of the lattice. Both the in-plane (anisotropic) and out-of-plane (isotropic) response have been examined and used in understanding the mechanism of oxidation on this surface. The study shows that

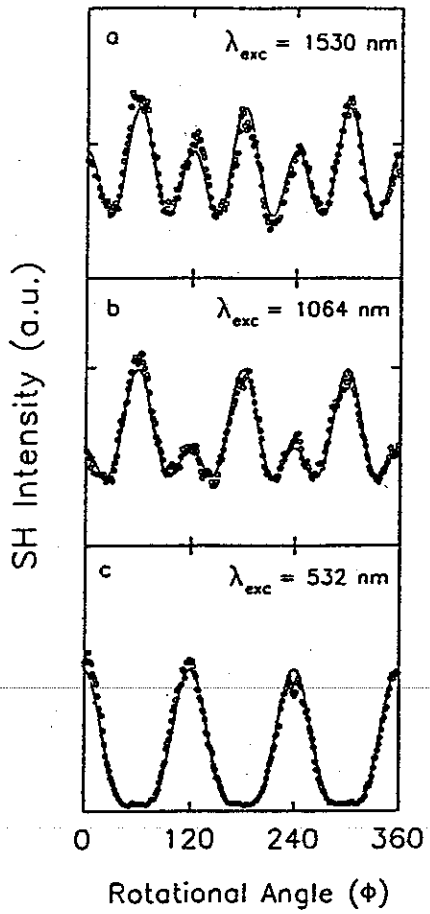

Fig. 14. SH intensity from Au(111) electrode surface at the PZC as a function of rotational angle, under *p*-in and *p*-out condition at the incident wavelength of (a) 1530 nm, (b) 1064 nm, and (c) 532 nm. The fits for $c^{(3)}/a^{(\infty)}$ are $-0.9e^{i82^\circ}$, $-1.1e^{i70^\circ}$, and $0.9e^{i0^\circ}$ respectively. From Ref. 51.

SHG is sensitive to the various stages of oxidation, and provides a more detailed picture of the oxidation process than can be extracted from the CV data.

Both the Au(100) and the Au(111) surfaces were examined in studies aimed at measuring the relative surface/bulk response from gold surfaces.[37] For the Au(100) surface and a *p*-polarized incident pulse at 1064 nm, anisotropy in the *p*- and *s*-polarized responses were found to be minimal. The potential-dependence for this surface was also examined. The *p*-polarized response was found to increase by a factor of 4 when the voltage was swept positive of the PZC from −0.1 V to +0.8 V. The *s*-polarized

response which was very small and isotropic showed no change with bias voltage. All of the data from this surface are consistent with a dominance of the surface response relative to the bulk at these nonresonant wavelengths.

4.2.2. *Surface Reconstruction*

Au(111) is an interesting system for study, not only for its electronic properties, but its ability to reconstruct in UHV. Both clean Au(111) and Au(100) have been known to reconstruct in UHV. Surface reconstruction occurs when the surface atoms of a solid rearrange themselves in a structure different from that expected from simple termination of the bulk lattice. Various studies by Kolb using cyclic voltammetry, electroreflectance spectroscopy and *ex situ* electron diffraction have suggested that flame-treated crystals form stable reconstructions in solution.[61,62] In more recent SH studies by Kolb and coworkers,[63] a change in the symmetry in the SH anisotropy has been observed for both of these crystals in regions where previous studies have suggested that the reconstruction occurs. Figure 15 shows the rotational anisotropy that they obtained for Au(111) at two different electrode potentials. Figure 15(a) corresponds to a freshly prepared (flame-treated) surface which was immersed at −0.4 V (vs. SCE) and then potentiostated at −0.1 V. Under these conditions, the Au(111) has been presumed to be reconstructed into the (1 × 23) structure where the surface atoms show a 4% compression in the [110] direction. The pattern appears to be one-fold in symmetry with two dominant peaks at 90° and 270° with the other four peaks markedly reduced in intensity. The authors fit the data to a mixture of one-fold and three fold symmetry elements. The observations are distinctly different when the electrode is ramped negatively. The data in Fig. 15 (b) was collected after the electrode in the above figure was biased at +0.7 V. In the figure, the threefold symmetry of the unreconstructed Au(111) - (1 × 1) surface is observed. Both sets of data were collected with *s*-polarized incident light at 1064 nm and the *s*-polarized output at 532 nm. Transient SH signals collected at an azimuthal angle of 90° indicate that the lifting and re-establishment of the reconstruction followed first-order kinetics with respective decay times of 22.7 s and 15.3 s. These reconstructions have also been studied in a series of electrolytes.

The more in depth analysis of the SH reconstruction data of Kolb and coworkers[63] on Au(111) has recently been performed by Lupke *et al.*[64] In this work, the second-order susceptibility tensor has been split into contributions due to 1-fold, 2-fold, 3-fold and ∞-fold axes for a surface of C_s

symmetry. Their results suggest that the SH rotational patterns cannot be completely analyzed by theoretical models without knowledge of the distribution of domains present in the reconstruction of the surface. They also conclude that rotation axes of lower symmetry create additional contributions via "overtones" or "harmonics". Their symmetry analysis of the SH rotational patterns from Au(111) reveals contributions from a 3-fold axis with a regular (1×1) structure and simultaneously from a 1-fold and a 2-fold axis due to the (1×23) reconstruction. Other studies of the effect of halide absorption on the reconstruction have also been reported.[65]

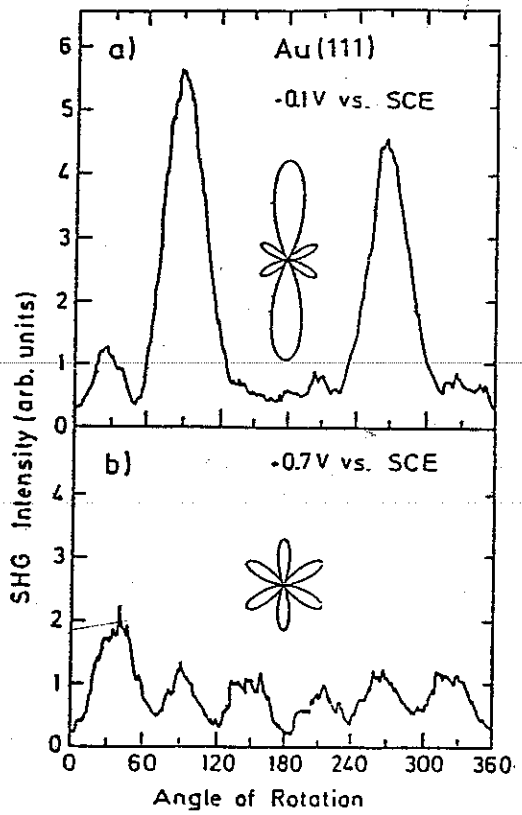

Fig. 15. SH intensity at 532 nm as a function of rotation angle for Au(111) in 0.01 M H_2SO_4 at (a) -0.1 V and (b) $+0.7$ V vs SCE. *S*-polarized excitation and *s*-polarized SHG detection in both cases. For comparison purposes the calculated polar plots of the rotational anisotropies for *s*/*s*-polarization of a threefold symetry surface with (a) and without (b) a onefold symmetry superimposed are also shown. From Ref. 61.

Au(100) offers another interesting case for reconstruction.[63] Previous studies on this electrode surface with LEED and RHEED have shown that

the reconstructed Au(100)–5 × 20 surface is stable in a potential range where no anion adsorption is present. In the presence of anions, the reconstruction is presumed to be lifted to a (1 × 1) structure. However, at negative potentials, the (5 × 20) structure is regenerated. The authors observed a difference in the SH rotational anisotropy at these two potentials and attributed it to the reconstruction and lifting of the reconstruction.[63]

4.2.3. *Underpotential Deposition*

Underpotential deposition of a foreign metal on Au(111) has been examined in several studies by Koos *et al.* (Ref. 60). In the first study by Koos using *p*-polarized 1064 nm incident light and detecting the *s*-polarized harmonic, the anisotropy which appeared with 3m symmetry initially is reduced after UPD of one monolayer. With the continued deposition to two monolayers, the anisotropic response increases to a level approximately equal to that of the adsorbate-free surface. The author suggested that the decrease in the anisotropic response is due to a lack of long range order upon the formation of an incommensurate overlayer.

A second study has examined changes in the phase of the SH response during overlayer deposition.[66] The experiment involved examining the *s*-polarized response from this (111) surface which allows isolation of the term $c(\chi^{(2)}_{xxx} - a\zeta)$, where a and c represent Fresnel factors and ζ is the nonlocal bulk response. The phase was then measured by the interference method. The results show that as the magnitude of the SH response decreases and passes through a minimum at $\Theta = 0.6$ ML, the relative phase of $c(\chi^{(2)}_{xxx} - a\zeta)$ is seen to shift 180° relative to that from the native surface. The authors attribute the initial phase shift to a possible flipping of the dipole at the surface. As the second layer forms, an increase in magnitude is observed as is a phase shift of −258°. The measured phase changes show distinct alterations in the nonlinear response at lower coverages which do not occur as higher coverages are attained. These differences are not obvious if only intensity measurements are made. The studies demonstrate the importance in making such complementary phase measurements.

A more recent study has examined the SH response from Au(111) electrodes during UPD of a variety of metals, Ag, Cu, Pb, Tl and Sb.[60] The lattice mismatch between lead and the substrate is shown to prevent formation of a commensurate overlayer but forms a hexagonal close-packed overlayer contracted by 0.7% from bulk lead. Although Tl and Sb on Au(111)

have not been examined by X-ray diffraction, a close packed structure would necessitate an incommensurate overlayer due to the lattice mismatch. Quite interestingly, the 3m symmetry is found by these studied to be retained for all of the metal overlayer/Au(111) systems even though there is a significant mismatch in the lattice parameters for the larger adatoms, thallium, antimony, and lead. However, by selectively monitoring the in-plane and out-of-plane response during each of the depositions, the authors show that indeed that depositions are very different for the adatoms which can align with the lattice relative to those which are lattice mismatched. The results are discussed in terms of the electronic structure of the Au(111) surface and the domain structures of the overlayers.

4.3. *Cu(111) and Cu(100)*

4.3.1. *Native Surface Studies*

The SH rotational anisotropy from a native Cu(111) electrode has been examined in several studies. The first of these by Shannon *et al.*[67] showed that with 1064 nm excitation, the native surface produces a response consistent with a three-fold symmetric interfacial region. The anisotropy is in qualitative agreement with results of Tom and Aumiller[68] for Cu(111) in UHV. More recently, Richmond and workers[23,54] have completed a more detailed study of the native copper electrode surface. In addition to examining the wavelength- and potential-dependence in the SH response, they have performed experiments in UHV on the same crystal to determine directly how the surface is perturbed by the presence of the solution. They find that even when the surface is biased at the PZC where the effect of the double layer should be a minimal, that although the symmetry of the interface is preserved, the rotational anisotropy is measurably different than found for Cu(111) in UHV. Figure 16 shows a cyclic voltammogram of Cu(111) in 0.01 M $HClO_4$ at pH 2. The CV reveals two clearly distinguishable anodic (a) and cathodic (c) peaks which have been associated with the respective formation and reduction of an oxygen containing surface film. Figure 17 shows the rotational anisotropies which result at various potentials within this potential region. All the data taken with 1064 nm *p*-polarized incident light and *p*-polarized SHG show C_{3v} symmetry but with varying phase angles between the isotropic and anisotropic contributions. The results are discussed in terms of the various surface species present

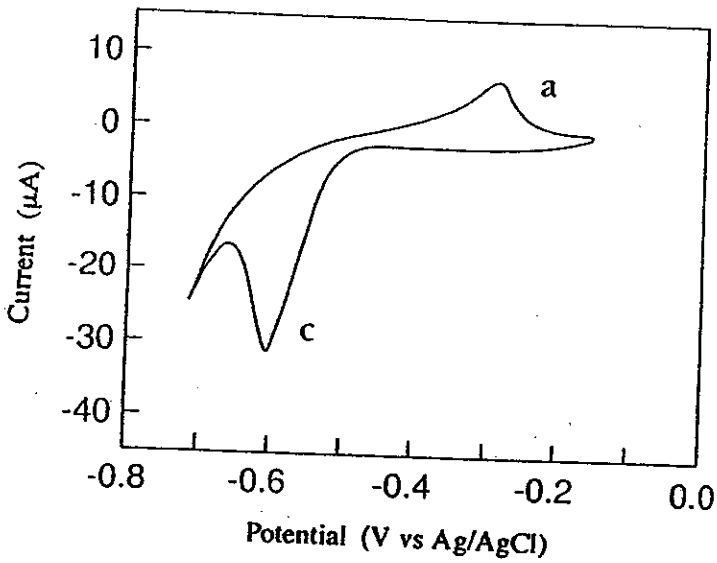

Fig. 16. Cyclic voltammogram of Cu(111) in 0.01 M $NaClO_4$ (pH 4) at a scan rate of 20 mV/s. From Ref. 52.

at the various potentials. The supposition that the surface is never in the native state observed for Au(111) and Ag(111) is based on comparison with the surface studied in UHV which has been sputtered and annealed. Figure 18(a) shows the results for similar optical conditions as Fig. 17 but with the surface in UHV. These results are consistent with the first study of Cu(111) in UHV by Tom and Aumiller.[68] The rather large differences in the magnitude and phase angle of the rotational anisotropy for the two environments suggests that the surface electronic properties in solution are very different than in UHV. The closest agreement is observed from reduced surfaces at negative potentials where both the magnitude and the phase angle approach the value of the UHV measurement. They conclude that the difference in anisotropy from Cu(111) can only be explained by the presence of an adsorbed species in solution. The most likely adsorbate is an oxygen species which cannot only tie up electrons at the surface and subsequently decrease the out-of-plane polarization, but can also affect the in-plane response by altering the electronic structure. Previous studies have suggested that oxygen containing species might be present on the surface of copper throughout the double layer charging region, including at the PZC, even though there is not evidence of its presence in the voltammetry.[69] Support for this conclusion came from dosing the clean Cu(111) surface in

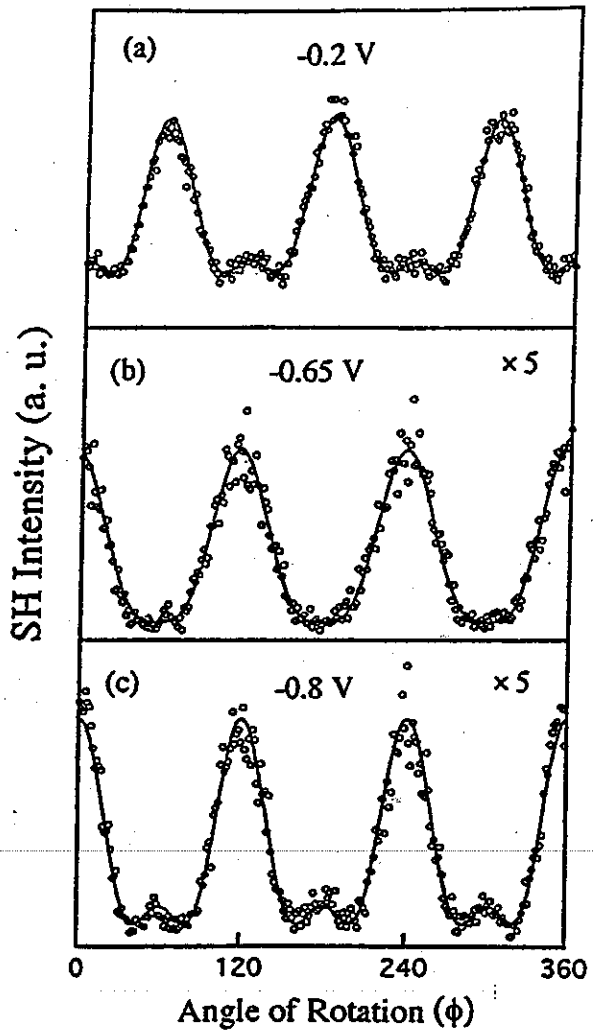

Fig. 17. SH rotational aniostropies from a Cu(111) electrode immersed in 0.01 M $NaClO_4$ at pH 4. *P*-input and output polarizations were used at the following fixed potentials: (a) −0.20 V vs Ag/AgCl, $c^{(3)}/a^{(\infty)} = 0.9e^{i121^\circ}$; (b) −0.65 V vs Ag/AgCl, $c^{(3)}/a^{(\infty)} = 0.77e^{i32^\circ}$; (c) −0.8 V vs Ag/AgCl, $c^{(3)}/a^{(\infty)} = 1.33e^{i44^\circ}$. The data is shown with open circles and the theoretical fit using Eq. (18) with solid lines. From Ref. 52.

UHV with increasing exposures to oxygen. The resulting oxygen containing surface gives an SH response which is more similar to that obtained in the electrochemical cell. [See Fig. 18(b)] Even with a wide variation of electrolyte solutions, potential and surface preparation, they were unable to attain an SH response from the submerged surface which could match that obtained in UHV.

The nonlocal response from Cu has been examined for Cu(100) in

experiments similar to those described for Ag(100) above.[37] The *s*-polarized SH intensities from either *p*- or *s*-polarized excitation at 1064 nm showed very low signal levels. Any response above the background did not vary periodically as the crystal was rotated. The authors concluded that the data is consistent with a dominance of the surface terms over the bulk at this incident and SH wavelength.

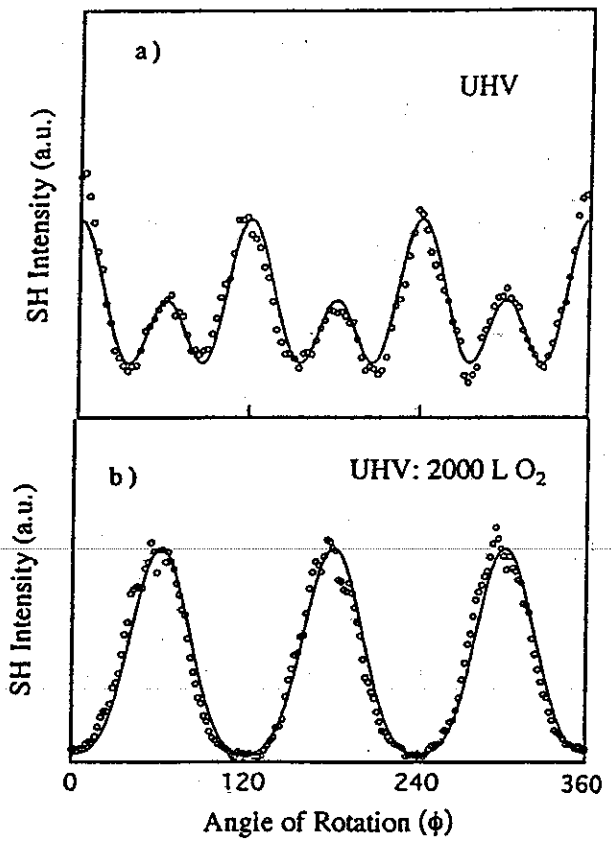

Fig. 18. SH rotational anisotropy from (a) a clean Cu(111) in UHV at 3.5×10^{-10} Torr, $c^{(3)}/a^{(\infty)} = 1.22e^{i77°}$, and (b) Cu(111) after exposure in UHV to 2000 L of O_2, $c^{(3)}/a^{(\infty)} = 0.8e^{i94°}$. The open circles represent the *p*-polarized incident and *p*-polarized SH data using 1064 nm excitation. Theoretical fits using Eq. (18) are indicated with a solid line. From Ref. 52.

4.3.2. *Wavelength-Dependent Studies*

The wavelength-dependence in the SH rotational anisotropy has been studied for Cu(111) in solution by Wong *et al.*[53,70] The results show that there is a strong wavelength-dependence between excitation with 532 nm, 1064 nm

and 1530 nm. As with Au(111) and Ag(111) there is a clear variation in the phase angle between the in-plane and out-of-plane response from 0 at the shorter wavelength to a much larger angle upon infrared excitation. The *d*-bands for Cu are near 2.0 eV which is in at least partial resonance with 1064 nm incident light. Since oxygen on the surface appears to be a factor in these studies also, the authors defer to the UHV measurements in drawing conclusions the important optical parameters involved describing the wavelength-dependence.

4.3.3. *Underpotential Deposition of Metallic Overlayers*

The earlier work of Shannon *et al.*[67] also examined the use of SHG to monitor the growth of Tl on Cu(111) to determine whether the underpotential deposited overlayer went onto the surface in an ordered or disordered manner. When thallium was deposited on this surface, the SHG indicated that the thallium overlayer grows in a disordered manner. It is interesting in retrospect to note that under their experimental conditions which included much care to reduce the presence of oxygen in solution, the thallium free surface displayed a rotational anisotropy similar to what Bradley *et al.*[23] later obtained for oxygen dosed Cu(111) in UHV. X-ray grazing incidence data by Materlin *et al.*[69] also suggests that thallium grows on the surface of Cu(111) in a disordered manner, largely due to the difficulty in producing an oxygen free substrate during electrodeposition in their grazing incidence cell. Later studies from this laboratory[23,71] in which the electrolytes used and the surface preparation lead to an SH rotational anisotropy closer to that of clean Cu(111) in UHV resulted in an SH anisotropy indicative of a relatively ordered overlayer growth on the surface. The later studies attribute this difference in overlayer structure from the earlier studies to different degrees of oxygen on the surface.[23]

4.3.4. *Time-Resolved Measurements*

A study of the temporal characteristics of thallium deposition on Cu(111) has been performed by Robinson and Richmond.[71] The experiments involved measuring the rotational anisotropy at various stages of deposition, followed by monitoring the time evolution of the deposition at a fixed rotation angle. A Nd:YAG mode-locked laser was used in these studies. Appropriate angles were chosen to allow the separate isotropic and anisotropic

temporal SH responses to be monitored. One of the interesting conclusions drawn from this study is that the time constant (τ) for adsorption of the first thallium overlayer depends on the final potential, E_f, of the potential step. They investigated the effect of underpotential and overpotential steps on the best-fit values of τ for exponential fits to $I_{p,p}(t)$. The under- and overpotentials, ΔE, are defined with respect to the maximum of the current peak, Ep, in the CV*s* for the first monolayer deposition. The time required to form the deposit increases at anodic potentials ($\Delta E < 0$) closest to Ep, indicating that more time is required to deposit successively larger coverages. The form of the data suggests that s would reach a maximum near $\Delta E = 0$. In the overpotential region, where the final coverage should be independent of E_f, the overlayer is formed faster as the overpotential increases. This result suggests that activation energy is supplied by the overpotential.

5. Summary

Detailed studies of the nonlinear response from single crystal metals examined in an electrochemical environment has provided important information about both the properties of the metal surface in a reactive environment and the source of the nonlinear optical response from metal surfaces under resonant and nonresonant conditions. The studies described demonstrate the important advantage of SHG for studying and comparing the properties of surfaces in a variety of environments. Many of the experiments have involved measuring the rotational anisotropy in the SH response from these crystalline surfaces. Such measurements are not only sensitive to the order and symmetry of the surface region but can provide valuable information about the relative phase of the response. The studies show that this relative phase of the in-plane and out-of-plane response can be highly sensitive to the electronic properties of the surface region. Under resonant conditions the phase is highly sensitive to surface electrostatics, incident wavelength and surface adsorbate. By monitoring the dispersion of the intensity and phase in this region, surface spectrosocopy can be achieved. Under nonresonant conditions for which current theoretical models would suggest the SH response should be is isotropic, anisotropy in the SHG with azimuthal rotation is strong. The phase of the response under these conditions can be adequately described by linear Fresnel theory. For studies of the geometrical structure of surfaces, the preference is to conduct such studies

under nonresonant conditions where phase changes due to alterations in the electronic structure can be minimized.

References

1. G. L. Richmond, J. M. Robinson, and V. L. Shannon, *Prog. in Surf. Sci.* **28**, 1 (1988).
2. G. L. Richmond, in *Electroanalytical Chemistry*, ed. A. J. Bard (Marcel Dekker, Inc., New York, 1991), p. 87.
3. G. L. Richmond, in *Modern Techniques for In Situ Characterization*, ed. H. Abruna (VCH, Brooklyn, NY, 1991), p. 267.
4. G. L. Richmond, in *Advances in Electrochemical Science and Engineering*, eds. H. Gerischer and C. W. Tobias (VCH Publishers, 1992).
5. P. N. Butcher and D. Cotter, *The Elements of Nonlinear Optics* (Cambridge University Press, Cambridge, 1990).
6. J. D. Jackson, *Classical Electrodynamics* (John Wiley & Sons, New York, 1975).
7. P. S. Pershan, *Phys. Rev.* **130**, 919 (1963).
8. P. Guyot-Sionnest and Y. R. Shen, *Phys. Rev.* **B38**, 7985 (1988).
9. D. A. Koos, *Optical Second Harmonic Generation Studies of Single Crystal Noble Metal Electrodes* (University of Oregon, 1991).
10. J. Reif, J. C. Zink, C. M. Schneider, and J. Kirschner, *Phys. Rev. Lett.* **67**, 2878 (1991).
11. Y. R. Shen, *The Principles of Nonlinear Optics* (Wiley, New York, 1984).
12. H. W. K. Tom, Ph.D. Thesis (University of California, Berkeley, 1984).
13. J. E. Sipe, D. J. Moss, and H. M. van Driel, *Phys. Rev.* **B35**, 1129 (1987).
14. M. H. Nayfeh and K. B. Morton, *Electricity and Magnetism* (John Wiley and Sons, New York, 1985).
15. J. O. Bockris and A. K. N. Reddy, *Modern Electrochemistry* (Plenum Publishing Corp., New York, 1977).
16. C. H. Lee, R. K. Chang, and N. Bloembergen, *Phys. Rev. Lett.* **18**, 167 (1967).
17. D. A. Koos, V. L. Shannon, and G. L. Richmond, *J. Phys. Chem.* **94**, 2091 (1990).
18. P. Guyot-Sionnest, A. Tadjeddine, and A. Liebsch, *Phys. Rev. Lett.* **64**, 1678 (1990).
19. R. D. Jones and P. R. Callis, *J. Appl. Phys.* **64**, 4301 (1988).
20. R. K. Chang, J. Duccing, and N. Bloembergen, *Phys. Rev. Lett.* **15**, 415 (1965).
21. K. Kemnitz, K. Bhattacharyya, J. M. Hicks, G. R. Pinto, and K. B. Eisenthal, *Chem. Phys. Lett.* **131**, 285 (1986).
22. R. A. Bradley, Ph.D. Dissertation, University of Oregon, 1992.
23. R. A. Bradley, K. A. Friedrich, E. K. L. Wong, and G. L. Richmond, *J. Electroanal. Chem.* **309(1-2)**, 319-24 (1991).
24. G. L. Richmond, *Langmuir* **2**, 132 (1986).

25. G. L. Richmond, *Chem. Phys. Lett.* **110**, 571 (1984).
26. V. L. Shannon, D. A. Koos, and G. L. Richmond, *J. Chem. Phys.* **87**, 1440 (1987).
27. V. L. Shannon, D. A. Koos, J. M. Robinson, and G. L. Richmond, in *Chemically Modified Surfaces* (Gordon and Breach Science Publishers, New York, 1988), p. 485.
28. H. M. Rojhantalab and G. L. Richmond, in *Advanced in Laser Science-II* eds. W. C. Stwalley, M. Lapp, and G. A. Kenney-Wallace (AIP, New York, 1987).
29. V. L. Shannon, J. M. Robinson, and G. L. Richmond, *Spectroscopy* **3**, 4 (1988).
30. V. L. Shannon, D. A. Koos, and G. L. Richmond, *J. Chem. Phys.* **87**, 1440 (1987).
31. R. A. Bradley *et al. Chem. Phys. Lett.* **168**, 468 (1990).
32. R. A. Bradley, R. Georgiadis, S. D. Kevan, and G. L. Richmond, *J. Vac. Sci. Tech.* **A10**, 2996 (1992).
33. R. A. Bradley, R. Georgiadis, S. D. Kevan, and G. L. Richmond, *J. Chem. Phys.* **99**, 5535 (1993).
34. V. L. Shannon, D. A. Koos, and G. L. Richmond, *J. Phys. Chem.* **91**, 5548 (1987).
35. V. L. Shannon, D. A. Koos, and G. L. Richmond, *Appl. Opt.* **26**, 3579 (1987).
36. V. L. Shannon, D. A. Koos, J. M. Robinson, and G. L. Richmond, *Chem. Phys. Lett.* **142**, 323–328 (1987).
37. D. A. Koos, V. L. Shannon, and G. L. Richmond, *Phys. Rev.* **B47**, 4730 (1993).
38. L. Laguren-Davidson, F. Lu, G. N. Salaita, and A. T. Hubbard, *Langmuir* **4**, 224 (1988).
39. E. D. Palik, *Handbook of Optical Constants of Solids* (Academic Press, Inc., New York, 1985).
40. F. Bassani, G. Pastori Parravincini, and R. A. Ballinger, *Electronic States and Optical Transitions in Solids* (Permagon Press Ltd., New York, 1975).
41. R. Georgiadis and G. L. Richmond, *J. Phys. Chem.* **95**, 2895 (1991).
42. R. Georgiadis, G. A. Neff, and G. L. Richmond, *J. Chem. Phys.* **92**, 4623 (1990).
43. H. M. Rojhantalab and G. L. Richmond, *J. Phys. Chem.* **93**, 3269 (1989).
44. A. Liebsch, *Phys. Scr.* **35**, 354 (1987).
45. A. Liebsch, *Phys. Rev. Lett.* **61**, 1233 (1988).
46. T. E. Furtak, L. J. Simpson, and Y. Tang, *Phys. Rev.* **B46**, 1719 (1992).
47. J. Schneider, C. Franke, and D. M. Kolb, *Surf. Sci.* **198**, 277 (1988).
48. L. E. Urbach, K. L. Percival, J. M. Hicks, E. W. Plummer, and H.-L. Dai, *Phys. Rev.* **B45**, 3769 (1992).
49. C. M. Li, L. E. Urbach, and H.- L. Dai, *Phys. Rev.* **B49** 2104 (1994).
50. Y. Tang, L. J. Simpson, and T. E. Furtak, *Phys. Rev. Lett.* **67**, 2814 (1991).
51. A. V. Petukhov, *Phys. Rev.* **B42**, 9387 (1990).

52. E. K. L. Wong, K. A. Friedrich, and G. L. Richmond, *Chem. Phys. Lett.* **195**, 628 (1992).
53. E. K. L. Wong and G. L. Richmond, *J. Chem. Phys.* **99**, 5500 (1993).
54. E. K. L. Wong, A. Friedrich, J. M. Robinson, R. A. Bradley, and G. L. Richmond, *J. Vac. Sci. Tech.* **A10**, 2985 (1992).
55. D. M. Kolb, *Ber. Bunsen-Ges. Phys. Chem.* **92**, 1175 (1988).
56. J. Miragliotta and T. E. Furtak, *Phys. Rev.* **B37**, 1028 (1988).
57. T. E. Furtak, J. Miragliotta, and G. M. Korenowski, *Phys. Rev.* **B35**, 2569 (1987).
58. J. Miragliotta and T. E. Furtak, *Surf. Interface Anal.* **14**, 53 (1989).
59. A. Friedrich and G. L. Richmond, *Ber. Bunsen-Ges. Phys. Chem.* **93**, 386 (1993).
60. D. A. Koos and G. L. Richmond, *J. Phys. Chem.* **96**, 3770–5 (1992).
61. D. M. Kolb and J. Schneider, *Electrochimica Acta* **31**, 929 (1986).
62. D. M. Kolb and J. Schneider, *Surf. Sci.* **162**, 764 (1985).
63. A. Friedrich *et al. Chem. Phys. Lett.* **163**, 123–8 (1989).
64. G. Luepke *et al. Phys. Rev.* **B41**, 6913 (1990).
65. A. Friedrich, C. Shannon, and B. Pettinger, *Surf. Sci.* **251–252**, 587 (1991).
66. D. A. Koos and G. L. Richmond, *J. Chem. Phys.* **93**, 869-72 (1990).
67. V. L. Shannon, D. A. Koos, S. A. Kellar, P. Huifang, and G. L. Richmond, *J. Phys. Chem.* **93**, 6434 (1989).
68. H. W. K. Tom and G. D. Aumiller, *Phys. Rev.* **B33**, 8818 (1986).
69. G. Materlik, M. Schmäh, J. Zegenhagen, and W. Uelhoff, *Ber. Bunsenges. Phys. Chem.* **91**, 292 (1987).
70. E. K. L. Wong, Ph.D. Thesis, Univ. of Oregon, 1992.
71. J. M. Robinson and G. L. Richmond, **10**, 2985 (in preparation).